Lithos 105 (2008) 301–318

Contents lists available at ScienceDirect

Lithos

journal homepage: www.elsevier.com/locate/lithos

High-pressure metamorphic rocks from Tongbaishan, central China: U–Pb and $^{40}Ar/^{39}Ar$ age constraints on the provenance of protoliths and timing of metamorphism

Xiaochun Liu [a,*], Bor-ming Jahn [b,c], Shuwen Dong [a], Yuxing Lou [d], Jianjun Cui [a]

[a] Institute of Geomechanics, Chinese Academy of Geological Sciences, Beijing 100081, PR China
[b] Institute of Earth Sciences, Academia Sinica, Taipei 115, Taiwan
[c] Department of Geosciences, National Taiwan University, Taipei 106, Taiwan
[d] School of Earth and Space Sciences, Peking University, Beijing 100871, PR China

ARTICLE INFO

Article history:
Received 6 November 2007
Accepted 28 April 2008
Available online 20 May 2008

Keywords:
U–Pb dating
$^{40}Ar/^{39}Ar$ dating
Yangtze basement
Permian–Triassic
HP metamorphism
Diachronous exhumation
Tongbaishan

ABSTRACT

The Tongbaishan area is situated at the junction between the Paleozoic North Qinling orogen and the Mesozoic South Qinling–Dabie–Sulu orogen. The area contains an important geological section for understanding the assembly of the Sino-Korean and Yangtze cratons. Two eclogite zones were recently recognized in this area. The peak metamorphic conditions are estimated to be 530–610 °C and 17–20 kbar for the northern eclogite zone and 460–560 °C and 13–19 kbar for the southern eclogite zone. SHRIMP U–Pb analyses on zircons of eclogite, metagabbro and orthogneiss indicate that their protoliths were formed during the Neoproterozoic, and experienced high-pressure (HP) recrystallization during the Permian–Triassic period. Therefore, the Tongbaishan area belongs to the western extension of the Dabieshan HP/UHP terrane. In addition, U–Pb ages of detrital zircons from quartzite, paragneiss and schist show three age populations of 2.49 Ga, 1.93 Ga and 1.85–1.82 Ga, suggesting that extensive Paleoproterozoic orogeny or tectonothermal events took place in the northern margin of the Yangtze craton. The SHRIMP dating and complementary $^{40}Ar/^{39}Ar$ dating of muscovite from quartzofeldspathic gneiss and quartzite reveal that the crustal rocks were subducted to great depths and underwent HP eclogite facies metamorphism at ca. 255 Ma, slightly earlier than the timing of deep subduction of the UHP slice. The HP rocks were later exhumed to mid- to upper-crustal levels and suffered from retrograde recrystallization at ca. 238 Ma. The dating also discloses a still later phase of deformation and recrystallization at ca. 215 Ma. The available age data throughout the Tongbai–Dabie–Sulu orogen reflect diachronous exhumation from ca. 238 Ma for the HP slice to ca. 213 Ma for the UHP slice. Such a phenomenon could be explained by successive subduction and exhumation of the broken slices of the subducting Yangtze slab.

1. Introduction

The Paleozoic–Mesozoic Qinling–Dabie–Sulu orogen marks the suture zone between the Sino-Korean and Yangtze cratons. The most important feature of the orogen is the preservation of high-pressure and ultrahigh-pressure (HP/UHP) metamorphic rocks of different ages. Regionally, Cambrian HP/UHP rocks occur in North Qinling (Qinling Group) (Hu et al., 1995, 1996; Yang et al., 2003a), whereas Triassic HP/UHP rocks are mainly distributed in the Dabieshan and Sulu areas (Hacker et al., 1996; Liou et al., 1996). Furthermore, some HP eclogites from the northwestern corner of western Dabieshan (i.e. Hong'an block) appear to have formed during the Silurian or Carboniferous time (Jian et al., 1997, 2000; Xu et al., 2000; Li et al., 2001; Sun et al., 2002). Since HP/UHP metamorphic rocks record the history of continental subduction, collision and subsequent exhumation, the multiple HP/UHP events registered in the Qinling–Dabie–Sulu orogen have well constrained the geodynamic evolution during the assembly of the Sino-Korean and Yangtze cratons.

The Tongbaishan area lies at the junction between the Paleozoic North Qinling orogen and the Mesozoic South Qinling–Dabie–Sulu orogen (Fig. 1). HP eclogites and their retrograde products have recently been recognized in several localities in this area (Wei et al., 1999; Suo et al., 2001; Liu et al., 2005). These rocks clearly holds key to the understanding of the evolution of the Qinling–Dabie–Sulu orogen, and therefore, geochronological data are most critical. Up to the present, however, the ages of these HP rocks remain unconstrained. In this paper, we report SHRIMP U–Pb ages on zircon and $^{40}Ar/^{39}Ar$ ages on muscovite

* Corresponding author. Institute of Geomechanics, Chinese Academy of Geological Sciences, 11 Minzudaxue Nanlu, Beijing 100081, PR China. Tel.: +86 10 68486756; fax: +86 10 68422326.
E-mail address: liuxchqw@yahoo.com.cn (X. Liu).

0024-4937/$ – see front matter © 2008 Elsevier B.V. All rights reserved.
doi:10.1016/j.lithos.2008.04.009

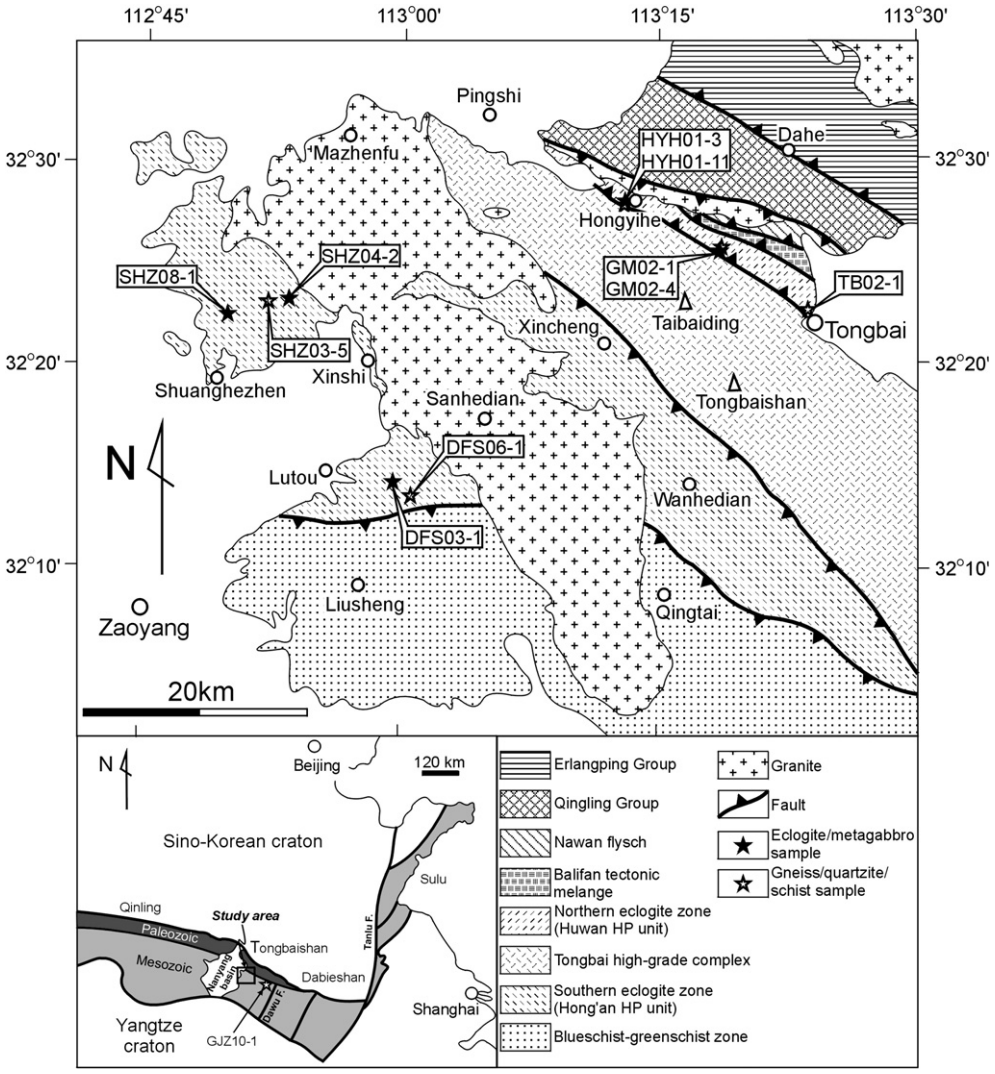

Fig. 1. Simplified geological map of the Tongbaishan area and its location in the Qinling–Dabie–Sulu orogen of China.

from metabasites (eclogite and metagabbro) and their country rocks (gneiss, quartzite and schist) from the Tongbaishan area in order to (1) delineate the formation time and provenance of protoliths of the HP rocks, and (2) to date the event of HP metamorphism. The geodynamic evolution between the Sino-Korean and Yangtze cratons will be further discussed in conjunction with the available age data from the Dabie–Sulu HP/UHP metamorphic terrane.

2. Regional geology and HP metamorphism

The Tongbaishan area is separated from Qinling in the west by the Nanyang basin, and from western Dabieshan in the east by the Dawu fault (Fig. 1). The area comprises three Paleozoic and five Mesozoic metamorphic units. These metamorphic units are separated by large-scale shear zones as a result of extensional detachment at a late stage of exhumation (Zhong et al., 1999, 2001; Suo et al., 2001). A major shear zone along the southwest boundary of the Tongbai complex (see below) has been dated at 131–119 Ma (Webb et al., 1999, 2001). In addition, numerous Cretaceous granitic plutons intruded in the metamorphic rocks during the extensional stage.

The three Paleozoic metamorphic units are represented, from northeast to southwest, by the Erlangping Group, the Qinling Group and the Nanwan flysch. The Erlangping Group is an ophiolite sequence, composed of mafic to intermediate metavolcanic and metaplutonic rocks, fine-grained clastic metasediments and chert with Cambrian–Silurian fossils (Kröner et al., 1993; Ratschbacher et al., 2003, 2006). The Qinling Group comprises felsic and mafic granulites, amphibolite, granitic gneiss, marble and subordinate metapelite. The lithological assembly likely represents a magmatic arc sequence accreted on to the Sino-Korean craton during the Ordovician–Silurian time (Kröner et al., 1993; Okay et al., 1993; Ratschbacher et al., 2003, 2006). The Nanwan flysch is limited to a narrow strip and consists of Devonian quartz sandstone, pelite and minor greywacke. These rocks were metamorphosed at the greenschist to epidote–amphibolite facies conditions, but their metamorphic age and tectonic significance remain unclear (Li et al., 2001; Ratschbacher et al., 2006).

The five Mesozoic metamorphic units are, from northeast to southwest, the Balifan tectonic mélange, the northern eclogite zone, the Tongbai high-grade metamorphic complex, the southern eclogite zone and the blueschist–greenschist zone. Except for the absence of a coesite-bearing eclogite zone, these metamorphic units seem to correspond one by one to those in western Dabieshan (Liu et al., 2004a,b). The Balifan tectonic mélange consists of highly strained granite, mylonitized quartzofeldspathic gneiss and epidote–amphibolite, with a strongly elongated metagabbro body. The northern eclogite zone, geographically identical to the Huwan HP unit (Liu et al., 2004a,b) or the Huwan shear zone (Hacker et al., 2000; Webb et al., 2001; Ratschbacher et al., 2003, 2006) of western Dabieshan,

Table 1
Sampling localities, mineral assemblages and age results of the dated rocks from the Tongbaishan area

Sample	Location	Coordinates	Lithology	Mineral assemblage	Age results (Ma)	
					U–Pb age	$^{40}Ar/^{39}Ar$ age
HYH01-3	Hongyihe	N 32°27′36″ E 113°13′14″	Eclogite	Grt+Omp+Amp+Phg+Ep+Qtz+Rt+Ilm	215±3	
GM02-1	Luozhuang	N 32°25′14" E 113°18′30"	Retrograde eclogite	Grt+Amp+Phg+Ep+Pl+Qtz+Rt+Ttn	255±6 216±14	
SHZ08-1	Dahekou	N 32°22′38" E 112°49′18"	Eclogite	Grt+Omp+Amp+Phg+Qtz+Rt	1645±15 257±16	
DFS03-1	Dafushan	N 32°13′52" E 112°58′41"	Metagabbro	Grt+Amp+Pg+Ep+Pl+Qtz+Rt	662±10 594±13	
HYH01-11	Hongyihe	N 32°27′36" E 113°13′14"	Quartzofeldspathic orthogneiss	Phg+Pl+Kfs+Qtz+Ilm	735±9	238±2
GM02-4	Luozhuang	N 32°25′16" E 113°18′34"	Quartzofeldspathic orthogneiss	Phg+Pl+Kfs+Qtz+Ilm		238±2
GJZ10-1	Xujialing	N 31°57′49" E 113°58′39"	Quartzofeldspathic orthogneiss	Phg+Pl+Kfs+Qtz+Ilm		217±1
TB02-1	Tongbai	N 32°22′24" E 113°23′18"	Pelitic schist	Grt+Phg+Pl+Qtz+Rt+Ilm	1820±6	
DFS06-1	Dafushan	N 32°13′18" E 113°00′18"	Quartzite	Phg+Pl+Qtz+Rt	2490±11 1930±7	234±2
SHZ03-5	Yaoyuan	N 32°22′56" E 112°51′56"	Quartzofeldspathic paragneiss	Grt+Phg+Pl+Qtz+Rt+Ttn	1846±5	337±2

Mineral abbreviations: Amp = amphibole; Ep = epidote; Grt = garnet; Kfs = K-feldspar; Omp = omphacite; Phg = phengite; Pg = paragonite; Pl = plagioclase; Qtz = quartz; Rt = rutile; Ttn = titanite.

Table 2
SHRIMP U–Pb analyses of zircons for high-pressure metamorphic rocks from the Tongbaishan area

Spot	U	Th	Th/U	Pb*	Common	Isotopic ratios			Ages (Ma)		CL domain
	(ppm)	(ppm)		(ppm)	^{206}Pb (%)	$^{206}Pb/^{238}U$	$^{207}Pb/^{235}U$	$^{207}Pb/^{206}Pb$	$^{206}Pb/^{238}U$	$^{207}Pb/^{206}Pb$	
Sample HYH01-3 (eclogite)											
1.1	1604	1347	0.87	52.2	0.07	0.0379±9	0.265±7	0.0508±7	240±6	232±32	Dark oscillatory-zoned core
1.2	170	136	0.82	5.81	0.32	0.0396±9	0.298±13	0.0547±20	250±5	400±83	Oscillatory-zoned rim
2.1	406	425	1.08	11.4	0.52	0.0327±7	0.233±11	0.0517±21	207±4	270±93	Oscillatory-zoned core
2.2	304	244	0.83	9.20	1.27	0.0348±8	0.205±19	0.0427±39	220±5		Oscillatory-zoned rim
3.1	928	521	0.58	24.3	0.17	0.0304±6	0.258±6	0.0616±9	193±4	661±32	Oscillatory-zoned rim
3.2	830	472	0.59	21.9	0.20	0.0306±6	0.209±6	0.0495±11	194±4	172±54	Oscillatory-zoned rim
4.1	132	247	1.93	13.2	0.21	0.1163±24	1.020±32	0.0636±15	709±14	729±48	Oscillatory-zoned core
5.1	506	474	0.97	14.5	0.06	0.0333±8	0.243±8	0.0528±11	211±5	322±45	Oscillatory-zoned core
5.2	559	599	1.11	17.3	0.77	0.0357±8	0.223±11	0.0453±19	226±5		Oscillatory-zoned rim
6.1	315	328	1.08	31.4	0.12	0.1162±23	1.018±25	0.0636±10	709±14	727±31	Oscillatory-zoned rim
6.2	213	259	1.25	23.2	0.20	0.1265±28	1.121±33	0.0643±12	768±16	751±38	Oscillatory-zoned rim
7.1	692	38	0.06	174	0.02	0.2923±58	4.522±90	0.1122±6	1653±29	1835±9	Grey homogeneous core
8.1	466	228	0.50	27.3	0.32	0.0679±16	0.519±15	0.0554±10	424±9	428±41	Oscillatory-zoned core
8.2	944	128	0.14	57.0	0.02	0.0702±14	0.540±13	0.0558±7	438±9	444±30	Oscillatory-zone rim
9.1	649	375	0.60	48.8	0.15	0.0875±19	1.043±44	0.0865±31	541±11	1349±70	Oscillatory-zoned core
11.1	338	408	1.25	32.7	0.23	0.1124±22	0.976±25	0.0630±10	686±13	709±35	Oscillatory-zoned core
12.1	484	355	0.76	43.6	0.36	0.1045±21	0.894±24	0.0621±11	641±12	676±37	Oscillatory-zoned rim
13.1	770	40	0.05	210	0.07	0.3171±63	4.99±11	0.1140±9	1775±32	1865±14	Grey cloudy-zoned rim
14.1	871	139	0.16	25.3	0.22	0.0337±7	0.235±7	0.0504±10	214±4	216±46	Oscillatory-zoned core
14.2	1753	188	0.11	51.5	0.08	0.0342±7	0.238±6	0.0504±6	217±5	216±29	Oscillatory-zoned rim
15.1	544	415	0.79	15.9	0.69	0.0338±7	0.244±10	0.0524±20	214±4	303±86	Oscillatory-zoned core
15.2	799	684	0.88	23.2	0.54	0.0336±7	0.229±10	0.0495±18	213±5	172±84	Oscillatory-zoned rim
Sample GM02-1 (retrograde eclogite)											
1.1	10	0	0.01	0.4	17.54	0.0396±21			250±19		Fir-tree-zoned core
1.2	20	0	0.01	0.9	20.60	0.0410±11			259±13		Fir-tree-zoned rim
2.1	8	2	0.19	0.4	33.04	0.0349±11			221±22		Fir-tree zoned mantle
2.2	12	1	0.12	0.4	4.11	0.0341±11			216±8		Fir-tree-zoned mantle
3.1	23	0	0.01	0.9	10.75	0.0406±10			257±9		Fir-tree-zoned core
3.2	2	0	0.01	0.2	88.01	0.0399±25			253±143		Fir-tree-zoned rim
4.1	7	0	0.05	0.4	42.76	0.0396±14			251±27		Fir-tree-zoned rim
5.1	15	0	0.03	0.7	15.58	0.0437±15			276±14		Fir-tree-zoned mantle
6.1	6	1	0.23	0.3	62.01	0.0333±16			211±32		Fir-tree-zoned rim
7.1	171	53	0.32	6.0	3.02	0.0404±8			255±5		Fir-tree-zoned rim
8.1	39	0	0.01	1.4	2.34	0.0410±9			259±6		Fir-tree-zoned rim
8.2	50	1	0.02	1.8	5.39	0.0397±8			251±6		Fir-tree-zoned rim
9.1	22	4	0.17	0.9	22.61	0.0399±10			252±9		Fir-tree-zoned core
Sample SHZ08-1 (eclogite)											
1.1	412	337	0.85	14.0	4.38	0.0380±6	0.300±33	0.0574±63	240±4	506±240	Oscillatory-zoned mantle
1.2	648	551	0.88	23.1	3.97	0.0399±6	0.300±30	0.0545±55	252±3	394±220	Oscillatory-zoned mantle

(continued on next page)

Table 2 (*continued*)

Spot	U	Th	Th/U	Pb*	Common	Isotopic ratios			Ages (Ma)		CL domain
	(ppm)	(ppm)		(ppm)	^{206}Pb (%)	^{206}Pb/^{238}U	^{207}Pb/^{235}U	^{207}Pb/^{206}Pb	^{206}Pb/^{238}U	^{207}Pb/^{206}Pb	
Sample SHZ08-1 (eclogite)											
2.1	185	150	0.83	20.0	3.00	0.1219±18	1.087±95	0.0647±56	742±11	764±180	Oscillatory-zoned rim
3.1	1786	985	0.57	84.1	2.41	0.0535±6	0.500±16	0.0678±20	336±4	862±61	Patchy core
4.1	812	689	0.88	189	0.41	0.2698±32	3.732±52	0.1003±8	1540±16	1630±15	Banded/patchy mixture
5.1	1815	1202	0.68	111	3.75	0.0685±8	0.693±28	0.0734±28	427±5	1025±78	Patchy core
6.1	2543	3186	1.29	437	0.08	0.2001±32	2.691±46	0.0976±4	1176±17	1578±8	Patchy core
7.1	2003	2070	1.07	185	0.43	0.1069±18	1.280±28	0.0868±12	655±11	1356±28	Patchy core
8.1	2687	3397	1.31	362	0.43	0.1563±25	2.077±37	0.0964±8	936±14	1555±16	Patchy core
9.1	3872	8926	2.38	366	2.05	0.1079±17	1.236±43	0.0831±26	661±10	1271±61	Patchy core
10.1	3153	4541	1.49	163	1.10	0.0595±10	0.552±17	0.0673±18	373±6	848±56	Patchy core
11.1	2451	3305	1.39	374	0.09	0.1774±28	2.344±40	0.0958±6	1053±15	1544±12	Patchy core
12.1	1553	1801	1.20	149	0.43	0.1111±18	1.320±29	0.0861±12	679±11	1341±27	Patchy core
13.1	1117	726	0.67	140	1.27	0.1438±27	1.886±60	0.0952±24	866±16	1531±48	Patchy core
14.1	1999	544	0.28	144	0.47	0.0835±13	0.943±22	0.0819±14	517±8	1243±34	Patchy core
15.1	3898	7289	1.93	491	0.49	0.1460±23	1.790±32	0.0889±9	879±13	1402±19	Patchy core
16.1	3038	5168	1.76	512	0.27	0.1958±31	2.605±44	0.0965±7	1153±16	1557±13	Patchy core
Sample DFS03-1 (metagabbro)											
1.1	257	528	2.13	21.7	0.26	0.0982±23	0.794±25	0.0586±13	604±13	554±49	Oscillatory-zoned core
2.1	168	71	0.44	14.3	2.36	0.0966±24	0.86±11	0.0647±78	595±14	763±260	Bright oscillatory-zoned core
3.1	858	1847	2.23	74.9	0.03	0.1016±21	0.854±20	0.0609±8	624±13	636±23	Dark oscillatory-zoned core
4.1	139	168	1.25	12.8	0.22	0.1071±26	0.896±38	0.0607±21	656±15	629±21	Bright oscillatory-zoned core
6.1	493	842	1.76	44.6	0.03	0.1053±23	0.895±30	0.0617±16	645±13	663±55	Oscillatory-zoned core
7.1	476	535	1.16	38.9	0.53	0.0945±24	0.815±28	0.0626±14	582±14	693±48	Oscillatory-zoned core
8.1	274	727	2.74	22.7	0.80	0.0956±36	0.790±55	0.0599±35	589±22	600±130	Oscillatory-zoned core
9.1	88	24	0.28	8.57	1.36	0.1122±29	0.989±61	0.0640±36	685±17	740±120	Bright oscillatory-zoned core
10.1	357	282	0.82	30.0	0.14	0.0979±34	0.805±31	0.0596±11	602±20	589±39	Oscillatory-zoned core
10.2	269	264	1.01	22.3	0.31	0.0961±33	0.831±33	0.0627±33	592±19	698±44	Oscillatory-zoned rim
11.1	357	790	2.28	33.0	0.20	0.1074±24	0.920±27	0.0621±11	658±14	679±39	Oscillatory-zoned rim
12.1	1298	936	0.74	122	0.07	0.1094±23	0.913±21	0.0605±6	669±13	623±21	Dark oscillatory-zoned rim
13.1	399	717	1.86	37.2	0.03	0.1085±24	0.924±23	0.0618±8	664±14	666±29	Oscillatory-zoned core
14.1	549	633	1.19	52.1	0.05	0.1103±24	0.941±24	0.0619±7	675±14	669±26	Oscillatory-zoned core
15.1	336	614	1.89	30.6	0.31	0.1058±25	0.853±28	0.0585±13	648±15	549±51	Oscillatory-zoned core
Sample HYH01-11 (quartzofeldspathic orthogneiss)											
1.1	342	386	1.17	34.2	0.09	0.1161±23	1.006±27	0.0628±11	708±14	702±37	Oscillatory-zoned rim
2.1	151	102	0.70	15.6	0.27	0.1203±28	1.079±33	0.0650±14	733±16	775±45	Oscillatory-zoned core
3.1	195	144	0.76	19.7	0.02	0.1174±25	1.039±27	0.0642±10	716±14	748±33	Oscillatory-zoned rim
4.1	251	231	0.95	25.9	0.25	0.1199±25	1.032±30	0.0624±12	730±14	689±43	Oscillatory-zoned core
4.2	206	188	0.95	21.6	0.00	0.1223±26	1.065±27	0.0632±9	744±15	714±30	Oscillatory-zoned rim
5.1	164	98	0.62	18.7	0.47	0.1319±28	1.134±40	0.0623±17	799±16	686±60	Oscillatory-zoned rim
6.1	115	74	0.66	12.5	0.31	0.1256±29	1.104±41	0.0637±18	763±17	733±59	Oscillatory-zoned core
7.1	348	482	1.43	36.7	0.08	0.1223±24	1.070±27	0.0634±9	744±14	722±29	Oscillatory-zoned core
8.1	1883	450	0.25	141	0.06	0.0871±17	1.031±46	0.0859±34	538±10	1335±77	Patchy-zoned core
9.1	254	242	0.98	26.6	0.11	0.1220±24	1.033±31	0.0614±13	742±14	654±46	Oscillatory-zoned core
10.1	1270	339	0.28	121	0.05	0.1108±22	0.998±21	0.0654±4	677±13	785±12	Patchy-zoned core
10.2	157	81	0.54	13.1	0.30	0.0971±21	0.935±30	0.0698±17	597±12	924±49	Oscillatory-zoned rim
11.1	1381	723	0.54	83.9	0.11	0.0706±14	1.044±29	0.1072±21	440±8	1753±36	Patchy-zoned core
12.1	90	45	0.51	8.24	0.13	0.1063±23	0.994±33	0.0679±17	651±14	864±52	Bright oscillatory-zoned core
13.1	191	364	1.97	19.9	0.22	0.1211±28	1.089±30	0.0652±10	737±16	782±32	Oscillatory-zoned core
14.1	265	348	1.36	28.1	0.15	0.1235±25	1.097±27	0.0644±10	751±14	756±32	Oscillatory-zoned core
15.1	310	261	0.87	27.4	0.35	0.1025±22	1.472±40	0.1041±18	629±12	1699±31	Oscillatory-zoned rim
16.1	76	47	0.64	7.79	0.00	0.1192±26	1.252±39	0.0762±16	726±15	1099±43	Bright oscillatory-zoned rim
17.1	246	148	0.62	23.6	0.21	0.1111±23	1.024±28	0.0668±11	679±13	831±36	Oscillatory-zoned rim
18.1	330	411	1.29	36.4	0.09	0.1281±28	1.108±28	0.0628±7	777±16	700±24	Oscillatory-zoned core
19.1	363	362	1.03	37.4	0.10	0.1196±24	1.059±24	0.0642±7	728±14	747±24	Oscillatory-zoned core
20.1	2171	367	0.17	137	0.06	0.0734±15	0.684±15	0.0676±5	457±9	855±16	Patchy-zoned core
21.1	225	155	0.71	21.9	0.29	0.1133±24	1.91±12	0.1223±76	692±13	1991±110	Oscillatory-zoned rim
22.1	250	333	1.38	23.2	0.09	0.1078±27	0.952±28	0.0640±9	660±16	743±29	Oscillatory-zoned core
23.1	151	155	1.06	15.4	0.05	0.1188±25	1.062±29	0.0649±10	723±15	770±34	Oscillatory-zoned core
24.1	291	352	1.25	29.5	0.05	0.1181±24	1.115±26	0.0685±8	720±14	883±24	Oscillatory-zoned rim
25.1	1689	226	0.14	117	0.04	0.0806±16	0.762±24	0.0686±17	500±10	885±52	Patchy-zoned core
Sample TB02-1 (pelitic schist)											
1.1	295	51	0.18	79.5	0.21	0.3132±81	4.80±13	0.1112±9	1757±40	1820±15	Grey sector-zoned core
2.1	222	10	0.04	66.9	0.14	0.3507±91	5.30±14	0.1097±9	1938±44	1794±15	Grey planar-zoned core
2.2	655	9	0.01	173	0.03	0.3076±80	4.70±12	0.1107±5	1729±39	1811±8	Bright homogeneous rim
3.1	1251	26	0.02	325	0.02	0.3023±76	4.75±12	0.1139±4	1703±38	1863±7	Grey planar/sector-zoned core
3.2	2097	49	0.02	512	0.01	0.2841±71	4.37±11	0.1116±3	1612±36	1825±5	Dark sector-zoned rim
4.1	792	93	0.12	242	0.04	0.3548±92	5.80±15	0.1186±6	1957±44	1936±9	Oscillatory-zoned core
5.1	241	11	0.05	68.5	0.15	0.3300±86	4.97±13	0.1092±10	1838±42	1785±16	Bright homogeneous rim
6.1	1723	26	0.02	458	0.04	0.3091±77	4.75±12	0.1114±7	1736±39	1823±11	Grey planar-zoned core
6.2	302	53	0.18	85.5	0.10	0.3298±86	5.03±14	0.1106±8	1837±41	1809±14	Bright homogeneous rim
7.1	796	36	0.05	213	0.11	0.3107±81	4.78±13	0.1115±6	1744±40	1824±10	Grey planar-zoned core
7.2	487	38	0.08	124	0.10	0.2961±77	4.45±12	0.1089±9	1672±38	1781±16	Grey planar-zoned core

Table 2 (*continued*)

Spot	U	Th	Th/U	Pb*	Common	Isotopic ratios			Ages (Ma)		CL domain
	(ppm)	(ppm)		(ppm)	^{206}Pb (%)	^{206}Pb/^{238}U	^{207}Pb/^{235}U	^{207}Pb/^{206}Pb	^{206}Pb/^{238}U	^{207}Pb/^{206}Pb	
Sample TB02-1 (pelitic schist)											
8.1	635	234	0.38	177	0.06	0.3241±84	5.15±13	0.1151±7	1810±40	1882±10	Oscillatory-zoned core
9.1	296	16	0.06	87.2	0.13	0.3426±89	5.23±14	0.1108±9	1899±43	1812±15	Bright homogeneous rim
10.1	338	33	0.10	93.1	0.12	0.3207±83	4.90±13	0.1108±7	1793±41	1812±12	Grey planar/sector-zoned core
11.1	569	65	0.12	157	0.12	0.3209±83	5.10±13	0.1153±6	1794±40	1884±10	Grey planar-zoned core
Sample DFS06-1 (quartzite)											
1.1	169	166	1.02	48.3	0.07	0.3327±70	5.41±12	0.1180±9	1851±33	1926±14	Oscillatory/sector-zoned rim
2.1	342	237	0.72	104	0.02	0.3527±71	5.74±12	0.1181±6	1947±34	1928±9	Oscillatory/sector-zoned core
2.2	391	460	1.21	107	0.02	0.3180±64	5.18±11	0.1182±6	1780±31	1930±9	Oscillatory/sector-zoned rim
2.3	424	280	0.68	108	0.03	0.2962±59	4.78±10	0.1169±6	1673±29	1909±9	Oscillatory/sector-zoned rim
3.1	143	141	1.02	43.0	0.03	0.3499±80	5.70±14	0.1183±12	1934±38	1930±18	Oscillatory/sector-zoned rim
4.1	156	154	1.02	48.6	0.04	0.3633±76	6.03±13	0.1203±9	1998±36	1961±13	Oscillatory/sector-zoned core
5.1	163	463	2.93	68.1	0.02	0.486±122	11.28±31	0.1683±16	2554±53	2541±16	Oscillatory/sector-zoned core
5.2	196	129	0.68	58.4	0.16	0.3462±73	7.74±23	0.1621±34	1916±35	2478±36	Grey homogeneous rim
6.1	166	61	0.38	68.3	0.01	0.480±101	10.99±23	0.1662±9	2526±43	2519±9	Oscillatory/sector-zoned core
6.2	125	31	0.26	50.8	0.05	0.473±114	10.61±27	0.1626±13	2497±50	2483±13	Grey homogeneous mantle
6.3	73	11	0.15	29.7	0.09	0.472±104	10.43±27	0.1605±22	2491±45	2460±24	Bright homogeneous rim
7.1	212	138	0.67	63.3	0.01	0.3476±70	5.71±12	0.1192±7	1923±34	1945±11	Oscillatory/sector-zoned core
8.1	139	52	0.39	40.6	0.05	0.3403±71	5.49±12	0.1171±9	1888±34	1912±14	Oscillatory-zoned core
9.1	233	171	0.76	76.3	0.17	0.3807±76	7.88±18	0.1502±15	2080±36	2348±17	Oscillatory-zoned core
9.2	222	161	0.75	53.2	0.00	0.2782±56	4.70±13	0.1225±23	1582±28	1994±34	Oscillatory/sector-zoned mantle
9.3	226	112	0.51	73.6	0.03	0.3786±76	6.21±14	0.1191±8	2070±36	1942±13	Oscillatory/sector-zoned rim
9.4	346	220	0.66	103	0.02	0.3462±69	5.64±12	0.1181±6	1916±33	1928±10	Oscillatory/sector-zoned rim
10.1	338	261	0.80	95.3	0.01	0.3279±72	5.65±13	0.1249±8	1828±35	2027±11	Oscillatory/sector-zoned core
11.1	38	28	0.76	9.64	0.59	0.2920±70	4.58±15	0.1139±26	1651±34	1862±41	Bright homogeneous core
11.2	301	119	0.41	90.6	0.00	0.3502±70	5.71±12	0.1183±7	1936±34	1930±10	Planar-zoned rim
12.1	272	77	0.29	137	0.05	0.586±117	13.33±29	0.1649±14	2974±49	2507±14	Grey homogeneous rim
12.2	240	58	0.25	96.3	0.01	0.4665±93	10.51±22	0.1635±7	2468±41	2492±7	Grey homogeneous rim
13.1	74	63	0.89	16.1	0.11	0.2550±56	4.50±12	0.1281±18	1464±29	2072±25	Bright oscillatory-zoned rim
Sample SHZ03-5 (quartzofeldspathic paragneiss)											
1.1	1418	276	0.20	359	0.04	0.2942±74	4.44±12	0.1095±3	1662±37	1792±6	Dark planar/sector-zoned core
2.1	284	216	0.78	106	0.13	0.436±113	8.73±24	0.1454±10	2331±51	2293±12	Oscillatory-zoned core
3.1	797	432	0.56	241	0.50	0.3500±91	7.13±19	0.1477±11	1934±43	2319±13	Oscillatory-zoned core
3.2	1445	407	0.29	268	0.63	0.2147±54	3.312±86	0.1119±6	1254±29	1830±10	Dark planar/sector-zoned rim
3.3	1759	645	0.38	320	0.70	0.2106±53	3.208±93	0.1105±15	1232±29	1807±25	Dark planar/sector-zoned rim
4.1	410	263	0.66	140	0.06	0.398±103	8.41±22	0.1534±6	2158±47	2384±7	Oscillatory-zoned core
5.1	348	64	0.19	101	0.36	0.3356±87	8.32±23	0.1798±15	1865±42	2651±13	Bright oscillatory-zoned core
5.2	1200	65	0.06	305	0.61	0.2937±73	4.62±13	0.1142±11	1660±37	1867±17	Grey planar-zoned mantle
5.3	1746	111	0.07	320	9.22	0.1934±50	2.69±15	0.1010±47	1140±27	1642±88	Dark planar-zoned rim
6.1	486	269	0.57	153	0.12	0.3659±95	6.26±17	0.1241±11	2010±44	2016±15	Oscillatory-zoned core
7.1	1315	1193	0.94	372	0.50	0.3281±82	7.38±19	0.1632±5	1829±40	2489±5	Dark oscillatory-zoned core
8.1	1993	870	0.45	202	16.10	0.0991±28	1.68±13	0.1232±89	609±16	2002±130	Dark oscillatory-zoned rim
9.1	1939	523	0.28	230	1.61	0.1357±34	1.654±46	0.0884±10	820±20	1391±21	Dark planar-zoned rim
10.1	527	133	0.26	126	0.46	0.2762±83	4.72±15	0.1239±7	1572±42	2013±11	Oscillatory-zoned core
11.1	574	356	0.64	120	1.08	0.2411±65	4.17±12	0.1254±13	1392±33	2034±18	Oscillatory-zoned core
12.1	370	398	1.11	147	0.08	0.4625±83	10.59±19	0.1661±8	2451±36	2518±8	Oscillatory-zoned core
13.1	154	128	0.86	57.1	0.18	0.4303±77	8.20±17	0.1383±14	2307±35	2206±17	Bright oscillatory-zoned core
14.1	425	153	0.37	181	0.17	0.4938±89	12.15±24	0.1785±18	2587±38	2639±17	Oscillatory-zoned core
15.1	776	129	0.17	280	0.05	0.4206±72	9.23±19	0.1591±19	2263±33	2447±21	Oscillatory-zoned core
16.1	1944	561	0.30	372	0.05	0.2226±38	3.342±60	0.1089±3	1296±20	1781±5	Dark planar/sector-zoned core
17.1	1943	562	0.30	394	0.09	0.2356±40	3.456±62	0.1064±4	1364±21	1739±8	Dark planar/sector-zoned core
18.1	146	61	0.43	61.4	0.15	0.4897±98	11.79±25	0.1746±9	2569±43	2602±9	Bright oscillatory-zoned core
19.1	1595	182	0.12	400	0.16	0.2912±50	4.530±82	0.1128±4	1647±25	1846±7	Grey planar/sector-zoned core
20.1	192	137	0.74	108	0.32	0.651±130	28.60±69	0.3186±45	3232±52	3563±21	Bright oscillatory-zoned core
21.1	93	40	0.45	46.6	0.12	0.582±175	15.14±61	0.1887±49	2957±71	2730±42	Bright oscillatory-zoned core
22.1	1137	92	0.08	297	0.03	0.3039±52	4.820±87	0.1150±4	1711±26	1880±6	Grey planar/sector-zoned core
23.1	1143	116	0.10	321	0.15	0.3259±55	5.104±92	0.1136±4	1818±28	1858±6	Grey planar/sector-zoned core
24.1	466	262	0.58	147	0.11	0.3673±66	6.64±12	0.1312±5	2017±30	2114±7	Oscillatory-zoned core
25.1	1141	91	0.08	272	0.18	0.2766±47	4.311±78	0.1131±6	1574±24	1849±9	Grey planar/sector-zoned core
26.1	1205	112	0.10	323	0.05	0.3121±53	4.871±88	0.1132±3	1751±27	1851±5	Grey planar/sector-zoned core
27.1	383	238	0.64	133	0.13	0.4032±73	7.65±14	0.1377±7	2184±33	2198±9	Bright oscillatory-zoned core
28.1	1233	125	0.10	335	0.09	0.3156±54	4.926±89	0.1132±5	1768±27	1851±9	Grey planar/sector-zoned core
29.1	1188	110	0.10	331	0.05	0.3243±55	5.025±90	0.1124±3	1811±27	1838±5	Grey planar/sector-zoned core
30.1	1473	184	0.13	349	0.12	0.2757±47	4.265±77	0.1122±4	1570±24	1835±6	Grey planar/sector-zoned core

Pb* denotes radiogenic Pb. Common ^{206} Pb (%) represents the proportion of common ^{206}Pb in total ^{206}Pb measured. Common Pb was corrected using the measured ^{204}Pb except for sample GM02-1 by assuming that ^{206}Pb/^{238}U and ^{208}Pb/^{232}Th ages are concordant. All uncertainties are 1σ.

comprises mylonitized granite, quartzofeldspathic gneiss, mica schist, marble and eclogite enclaves. The Tongbai high-grade metamorphic complex is dominated by granitic gneiss with minor supracrustal rocks characterized by quartzofeldspathic gneiss, marble and amphibolite. The protolith age of granitic gneiss was dated at ca. 750 Ma (Kröner et al., 1993), which was attributed to be the age of distinct magmatic event in the Yangtze craton (Hacker et al., 1998, 2000). However, whether or not this complex experienced HP

metamorphism is unclear. The southern eclogite zone, corresponding to the southern part of the Hong'an HP unit of western Dabieshan, consists of quartzofeldspathic gneiss and minor mica schist, quartzite and marble with numerous eclogite and garnet amphibolite lenses and several large metagabbro blocks. The blueschist–greenschist zone, equivalent to the Mulanshan unit of western Dabieshan, mainly comprises metamorphic bimodal volcanics and some metasedimentary rocks.

Eclogites from two eclogite zones commonly occur as lenses or blocks of a few to several hundreds meters size in quartzofeldspathic gneisses, mica schists and marbles. They have a similar mineral assemblage of garnet + omphacite + amphibole + phengite + quartz + rutile ± epidote. Some of them have subjected to retrograde overprinting at epidote–amphibolite facies conditions. Microprobe analyses reveal that all garnet grains are compositionally zoned, with an increase of pyrope, a decrease of spessartine and grossular and an irregular change of almandine from core to rim (Liu et al., 2005), suggesting a progressive growth of garnet. The *P–T* conditions of eclogite are estimated to be 530–610 °C and 17–20 kbar for the northern eclogite zone, and 460–560 °C and 13–19 kbar for the southern eclogite zone (Liu et al., 2005 and our unpublished data). The contrasting metamorphic conditions between the two zones demonstrate that they do not belong to the same portion of the HP slice, as different HP eclogite zones on the two sides of the UHP eclogite zone from western Dabieshan (Liu et al., 2004b).

3. Samples and analytical procedures

3.1. Sample description

In order to precisely define ages of protolith and HP metamorphism, two fresh eclogites (samples HYH01-3 and SHZ08-1), a retrograde eclogite (sample GM02-1), a metagabbro (sample DFS03-1), a quartzofeldspathic orthogneiss (sample HYH01-11), a quartzofeldspathic paragneiss (sample SHZ03-5), a pelitic schist (sample TB02-1) and a quartzite (sample DFS06-1) from the northern and southern eclogite zones were chosen for SHRIMP U–Pb zircon dating. Furthermore, samples HYH01-11, SHZ03-5, DFS06-1 and two other quartzofeldspathic orthogneisses (samples GM02-4 and GJZ10-1), which contain well-preserved muscovites, were selected for $^{40}Ar/^{39}Ar$ dating of muscovite. Their localities are shown in Fig. 1, and their coordinates, mineral assemblages and age results are presented in Table 1.

Samples HYH01-3 and SHZ08-1 are representative of eclogites taken from the northern and southern eclogite zones, respectively. The former occurs as a lenticular body (3 m wide and >5 m long) enclosed in quartzofeldspathic orthogneiss; the latter occurs as a large block of 100×270 m^2 in quartzofeldspathic paragneiss. The massive features may suggest that the protoliths of eclogites are gabbroic rocks. The retrograde eclogite (sample GM02-1) crops out as a long lens (ca. 10 m wide) in quartzofeldspathic orthogneiss from the northern eclogite zone. It consists of garnet, amphibole, phengite, epidote, plagioclase, quartz, rutile and titanite. Omphacite was only found as an inclusion in zircon. Sample DFS03-1 is from the weakly deformed domain of a large metagabbro block (12 km^2) from the southern eclogite zone. The magmatic texture is preserved in the block, but plagioclase was completely transformed to fine-grained zoisite + paragonite + albite, and clinopyroxene was replaced by amphiboles and rutile. Garnet coronas commonly occur around amphibole, but no omphacite was observed probably due to more calcic bulk composition of the rock.

Quartzofeldspathic ortho- and paragneisses are predominant rocks in both eclogite zones. All dated samples were taken away from the boundary faults of the eclogite zones. They show near-equigranular texture and strongly oriented foliation, with mineral grain sizes ranging from 0.5 to 1 mm. The mineral assemblage of orthogneiss samples HYH01-11, GM02-4 and GJZ10-1 is characterized by muscovite + plagioclase + K-feldspar + quartz + ilmenite, whereas paragneiss sample SHZ03-5 has an assemblage of garnet + muscovite + paragonite + plagioclase + quartz + rutile (only in garnet) + titanite. Sample DFS06-1 was collected from a quartzite layer of 15 cm thick in paragneiss. It contains more than 90% quartz and minor muscovite, plagioclase and rutile. The pelitic schist sample TB02-3 consists of garnet, muscovite, quartz and minor plagioclase, rutile and ilmenite. Muscovite in this sample was partially replaced by chlorite.

3.2. Analytical procedures

The U–Th–Pb zircon analyses were performed using the SHRIMP II sensitive high resolution ion microprobe at the Beijing SHRIMP Centre, Chinese Academy of Geological Sciences. Zircons were extracted from samples (one to several kilograms) using the conventional techniques, including crushing, sieving, heavy liquid and hand picking. Zircon grains were mounted in an epoxy disc along with the TEMORA zircon standard (416.75 ± 0.24 Ma; Black et al., 2003) and polished down to expose their centers. Internal structures of zircons were revealed by cathodoluminescence (CL) imaging. SHRIMP instrumental conditions and data acquisition procedures are the same as described by Williams (1998). A primary ion beam of 4.5 nA, 10 kV O_2^- and 25–30 μm spot were used. Mass resolution was ca. 5400 at 1% peak height. The data were collected in sets of five scans throughout the Zr, Pb, U and Th isotope species and a reference zircon was analyzed every two or three analyses. The measured $^{206}Pb/^{238}U$ ratios were corrected using reference zircon TEMORA. Ages and concordia diagrams were produced using the programs SQUID 1.03 (Ludwig, 2001a) and ISOPLOT 2.06 (Ludwig, 1999). Correction for common Pb was made by the measured ^{204}Pb, except for sample GM02-1 using ^{208}Pb correction because of the extremely low contents of U and Th in zircons. The decay constants used are: 0.155125 Ga^{-1} for ^{238}U, and 0.98485 Ga^{-1} for ^{235}U. The age uncertainties for individual analyses represent one standard deviation (1σ), but the calculated weighted mean $^{206}Pb/^{238}U$ or $^{207}Pb/^{206}Pb$ ages are quoted at 2σ. The analytical data are listed in Table 2.

The $^{40}Ar/^{39}Ar$ muscovite analyses were carried out using stepwise incremental heating method at the Institute of Geology, Chinese Academy of Geological Sciences. Instrumental conditions and analytical details were

Table 3
Representative microprobe analyses of muscovites for quartzofeldspathic gneiss and quartzite from the Tongbaishan area

Sample	HYH01-3		GM02-4		GJZ10-1		DFS06-1		SHZ03-5	
Domain	Core	Rim	Core	Rim	Core	Rim	Core	Rim	Core	Rim
SiO_2	46.79	46.46	49.76	49.93	47.12	47.57	49.76	49.80	48.74	48.63
TiO_2	0.40	0.58	0.26	0.32	1.15	1.01	0.6	0.58	0.47	0.52
Al_2O_3	33.39	32.82	25.90	26.01	24.09	23.23	27.43	27.54	30.81	30.48
Cr_2O_3	–	–	–	–	–	0.01	–	–	0.01	0.02
FeO*	2.96	2.98	5.37	5.56	8.69	9.16	2.49	2.57	2.17	2.13
MnO	0.08	0.04	0.08	0.01	0.14	0.28	–	–	0.06	0.03
MgO	0.36	0.41	2.10	2.11	1.83	1.90	2.92	2.79	2.06	2.16
CaO	0.02	–	–	0.01	–	–	–	–	0.02	0.02
Na_2O	0.59	0.19	0.10	0.09	0.05	0.08	0.23	0.24	0.88	0.95
K_2O	10.31	10.85	11.22	11.18	11.02	10.97	11.11	10.91	10.09	9.90
Total	94.90	94.33	94.79	95.22	94.09	94.21	94.54	94.43	95.31	94.84
Si	3.148	3.153	3.407	3.404	3.328	3.364	3.37	3.368	3.251	3.257
Ti	0.020	0.030	0.013	0.016	0.061	0.054	0.03	0.030	0.024	0.026
Al	2.646	2.623	2.088	2.088	2.004	1.935	2.18	2.193	2.420	2.404
Cr	–	–	–	–	–	0.001	–	–	0.001	0.001
Fe^{2+}	0.167	0.169	0.307	0.317	0.513	0.542	0.14	0.145	0.121	0.119
Mn	0.005	0.002	0.005	0.001	0.008	0.017	–	–	0.003	0.002
Mg	0.036	0.041	0.214	0.214	0.193	0.200	0.29	0.281	0.205	0.216
Ca	0.001	–	–	0.001	–	–	–	–	0.001	0.001
Na	0.077	0.025	0.013	0.012	0.007	0.011	0.03	0.031	0.114	0.123
K	0.885	0.939	0.980	0.972	0.993	0.990	0.96	0.941	0.859	0.846
Mg/(Fe+Mg)	0.18	0.20	0.41	0.40	0.27	0.27	0.68	0.66	0.63	0.64
Na/(Na+K)	0.08	0.03	0.01	0.01	0.01	0.01	0.03	0.03	0.12	0.13

*Total iron as FeO. – = not detectable. Formula is based on 11 O.

Table 4
$^{40}Ar/^{39}Ar$ analyses of phengites for quartzofeldspathic gneiss and quartzite from the Tongbaishan area

Step	T (°C)	$^{36}Ar/^{39}Ar$	$^{37}Ar/^{39}Ar$	$^{38}Ar/^{39}Ar$	$^{40}Ar/^{39}Ar$	^{39}Ar (cumulative) (%)	^{39}Ar ($\times 10^{-14}$ mol)	$^{40}Ar/^{39}Ar$	Ages (Ma)
Sample HYH01-11 (sample mass=60 mg; J-value=0.011956)									
1	400	0.0532	0.1219	0.0355	25.0080	0.10	35.51	9.3029	190±11
2	500	0.0346	0.4945	0.0304	17.2050	0.17	26.94	7.0194	145±10
3	600	0.0172	0.0382	0.0157	14.4284	0.42	92.84	9.3506	191.2±6.1
4	700	0.0128	0.0154	0.0151	13.6204	1.47	389.09	9.8463	200.8±2.2
5	800	0.0040	0.0082	0.0136	12.2239	3.86	884.53	11.0277	223.4±3.2
6	880	0.0013	0.0036	0.0150	10.0656	10.39	2413.35	11.6642	235.5±2.3
7	930	0.0005	0.0016	0.0134	11.8221	21.59	4143.61	11.6774	235.8±2.2
8	980	0.0003	0.0034	0.0135	11.9541	46.13	9072.26	11.8726	239.5±2.3
9	1030	0.0003	0.0034	0.0124	12.0539	67.51	7907.98	11.9500	240.9±2.5
10	1080	0.0004	0.0047	0.0125	11.9167	81.59	5206.42	11.7996	238.1±3.0
11	1140	0.0007	0.0029	0.0139	12.1290	90.36	3244.83	11.9304	240.5±3.4
12	1200	0.0006	0.0068	0.0185	12.0590	96.02	2092.57	11.8666	239.3±2.8
13	1300	0.0006	0.0046	0.0137	12.0088	99.28	1205.18	11.8362	238.8±2.3
14	1400	0.0043	0.0550	0.0144	13.0392	100.00	265.67	11.7677	237.5±2.3
Sample GM02-4 (sample mass=60 mg; J-value=0.011731)									
1	400	0.0230	0.2624	0.0489	18.2869	0.04	14.62	11.5146	229±10
2	500	0.0216	0.0574	0.0258	15.4133	0.20	65.14	9.0409	181.8±3.5
3	600	0.0110	0.0820	0.0167	12.4791	0.44	96.63	9.2393	185.6±3.8
4	700	0.0032	0.0156	0.0135	11.8312	1.11	270.88	10.8790	216.7±2.2
5	800	0.0017	0.0082	0.0166	11.8057	3.63	1017.94	11.2856	224.3±2.2
6	880	0.0011	0.0025	0.0124	11.8692	10.18	2643.74	11.5363	229.0±2.4
7	930	0.0007	0.0031	0.0125	11.9469	16.94	2730.54	11.7303	232.6±2.0
8	980	0.0006	0.0038	0.0151	12.3001	33.18	6557.31	12.1308	240.0±2.5
9	1030	0.0002	0.0009	0.0124	12.0419	82.92	20079.13	11.9716	237.1±2.8
10	1080	0.0004	0.0050	0.0128	12.1054	95.33	5010.67	11.9832	237.3±2.3
11	1130	0.0004	0.0069	0.0129	12.1345	99.05	1498.88	12.0075	237.7±2.5
12	1200	0.0014	0.0316	0.0149	12.4132	99.46	169.20	12.0044	237.7±3.2
13	1400	0.0101	0.0870	0.0147	14.9486	100.00	216.03	11.9607	236.9±2.6
Sample GJZ10-1 (sample mass=63 mg; J-value=0.011451)									
1	400	0.0743	0.2886	0.0336	28.9850	0.37	127.13	7.0572	140.2±4.7
2	500	0.0795	0.0872	0.0309	31.1509	1.06	240.13	7.6718	151.9±3.3
3	600	0.0532	0.0490	0.0238	25.1539	2.04	342.75	9.4188	184.8±3.1
4	700	0.0207	0.0152	0.0171	16.4422	3.93	655.23	10.3113	201.3±2.1
5	800	0.0030	0.0070	0.0135	11.7442	9.83	2055.23	10.8483	211.2±2.2
6	880	0.0009	0.0051	0.0128	11.4458	20.18	3598.68	11.1785	217.3±2.2
7	930	0.0006	0.0009	0.0128	11.3061	28.14	2767.24	11.1164	216.2±2.2
8	980	0.0007	0.0046	0.0134	11.4277	49.08	7285.76	11.2282	218.2±2.1
9	1030	0.0006	0.0025	0.0129	11.4302	74.86	8966.58	11.2350	218.3±2.2
10	1080	0.0007	0.0067	0.0117	11.4241	87.72	4473.02	11.2116	217.9±2.1
11	1130	0.0005	0.0020	0.0118	11.3747	95.96	3863.62	11.2129	217.9±2.1
12	1200	0.0006	0.0065	0.0133	11.3847	99.06	1080.27	11.1976	217.6±2.3
13	1300	0.0017	0.0422	0.0141	11.6552	99.68	215.22	11.1439	216.7±2.3
14	1400	0.0094	0.0524	0.0154	13.9066	100.00	110.67	11.1238	216.3±2.4
Sample DFS06-1 (sample mass=60 mg; J-value=0.011632)									
1	400	0.0798	0.3465	0.0406	34.0972	0.13	47.46	10.5472	208.8±8.8
2	500	0.0592	0.2620	0.0274	26.4631	0.25	48.05	8.9869	179.4±7.6
3	600	0.0471	0.1083	0.0235	23.9786	0.50	95.63	10.0633	199.7±8.5
4	700	0.0211	0.0190	0.0215	17.1653	1.51	382.34	10.9189	215.7±5.3
5	800	0.0064	0.0152	0.0141	13.5528	3.26	664.06	11.6654	229.5±3.4
6	880	0.0023	0.0055	0.0142	12.7180	9.77	2464.91	12.0372	236.4±2.2
7	930	0.0010	0.0047	0.0153	12.3902	18.66	3371.33	12.0829	237.2±2.2
8	980	0.0005	0.0019	0.0133	12.0020	28.20	3616.00	11.8544	233.0±2.9
9	1030	0.0003	0.0011	0.0134	11.7885	61.60	12663.20	11.6873	229.9±2.8
10	1080	0.0005	0.0091	0.0124	11.8908	75.24	5170.09	11.7397	230.9±2.9
11	1140	0.0005	0.0023	0.0124	11.9285	92.96	6720.13	11.7747	231.6±3.1
12	1200	0.0008	0.0059	0.0142	12.0468	96.88	1484.48	11.8105	232.2±2.4
13	1300	0.0011	0.0112	0.0130	12.3177	98.91	769.42	12.0015	235.7±2.3
14	1400	0.0102	0.0175	0.0137	15.0072	100.00	414.51	12.0026	235.8±2.8
Sample SHZ03-5 (sample mass=60 mg; J-value=0.01201)									
1	400	0.0386	0.1574	0.0279	22.3307	0.06	21.47	10.9410	223±14
2	500	0.0471	0.5089	0.0268	25.1088	0.11	15.29	11.2331	228±12
3	600	0.0200	0.1314	0.0196	19.3459	0.27	55.47	13.4474	270.1±8.4
4	700	0.0044	0.0176	0.0152	18.3458	0.91	217.30	17.0482	336.0±4.0
5	800	0.0018	0.0153	0.0129	17.6582	2.62	577.79	17.1342	337.6±3.5
6	880	0.0010	0.0035	0.0117	17.3298	7.01	1491.05	17.0261	335.6±3.5
7	940	0.0007	0.0043	0.0151	17.1129	23.67	5648.64	16.9044	333.4±3.1
8	1000	0.0003	0.0017	0.0127	17.3830	59.73	12227.92	17.2823	340.2±3.5
9	1050	0.0004	0.0027	0.0126	17.4788	77.27	5948.10	17.3578	341.6±3.4

(continued on next page)

Table 4 (*continued*)

Step	*T* (°C)	$^{36}Ar/^{39}Ar$	$^{37}Ar/^{39}Ar$	$^{38}Ar/^{39}Ar$	$^{40}Ar/^{39}Ar$	^{39}Ar (cumulative) (%)	^{39}Ar ($\times10^{-14}$ mol)	$^{40}Ar/^{39}Ar$	Ages (Ma)
Sample SHZ03-5 (sample mass=60 mg; J-value=0.01201)									
10	1100	0.0006	0.0131	0.0166	17.4080	91.00	4656.16	17.4080	339.1±3.8
11	1150	0.0006	0.0084	0.0143	17.3629	97.99	2372.10	17.1719	338.3±3.4
12	1220	0.0033	0.0205	0.0160	17.9459	99.41	481.10	16.9773	334.8±3.2
13	1300	0.0088	0.1304	0.0239	19.7679	99.75	116.31	17.1719	338.3±4.5
14	1400	0.0085	0.0846	0.0220	19.6614	100.00	83.37	17.1496	337.9±4.0

$^{40}Ar^*/^{39}Ar$ represents radiogenic $^{40}Ar/^{39}Ar$ ratio. Age uncertainties are 1σ.

described by Chen et al. (2002). The chemical compositions of muscovite were analyzed using a JEOL JXA-8000 wavelength-dispersive electron microprobe (Table 3). Muscovite concentrates were obtained using the conventional techniques (magnetic separators and heavy liquids) from the 70–114 μm size fraction for sample DFS06-1 and the 200–260 μm size fraction for four other samples. Muscovite for $^{40}Ar/^{39}Ar$ analysis was purified to >99% (except for sample SHZ03-5 with minor paragonite) and then ultrasonically cleaned in distilled water and ethanol. Samples were wrapped in aluminum foil and loaded into a tube of aluminum foil. Each tube contains 2–3 monitors (an internal standard: Fangshan biotite, 132.7±1.2 Ma; Chen et al., 2002) in between the minerals. A number of such tubes were sealed into quartz vial and irradiated for 2941 min in the nuclear reactor at the Chinese Academy of Atomic Energy. The reactor delivers a neutron flux of about 6.0×10^{12} n $cm^{-2}s^{-1}$; the integrated neutron flux is about 1.15×10^{18} n cm^{-2}. The irradiated samples and monitors were loaded into the vacuum extraction system and baked for 48 h at 120–150 °C. The Ar extraction system comprises an electron bombardment heated furnace in which the samples are heated under vacuum. The duration is 30 min for heating–extraction at each temperature increment, and 30 min for purification. The purified Ar was trapped in activated charcoal finger at liquid–nitrogen temperature, and then released into the MM-1200B Mass Spectrometer to analyze Ar isotopic ratios. Measured isotopic ratios were corrected for mass discrimination, atmospheric Ar component, procedural blanks and mass interference induced by irradiation. The blanks of m/e of ^{40}Ar, ^{39}Ar, ^{37}Ar and ^{36}Ar are less than 6×10^{-15}, 4×10^{-16}, 8×10^{-17} and 2×10^{-17} mol, respectively. The correction factors of interfering isotopes produced during irradiation were determined by the analysis of irradiated K_2SO_4 and CaF_4 pure salts. The values are: $(^{40}Ar/^{39}Ar)_k=0.004782$; $(^{36}Ar/^{37}Ar)_{Ca}=0.000240$; $(^{39}Ar/^{37}Ar)_{Ca}=0.000806$. Ages were calculated using the ISOPLOT program (version 2.49; Ludwig, 2001b). The K decay constant used was 0.5543 Ga^{-1}. All ^{37}Ar were corrected for radiogenic decay (half-life 35.1 days). Uncertainties on the apparent ages on each step are quoted at the 1σ level, but weighted mean plateau ages and isochron ages are given at the 2σ level. The analytical results are given in Table 4.

4. Geochronological results

4.1. SHRIMP U–Pb zircon ages

4.1.1. Sample HYH01-3: eclogite from the northern eclogite zone

Zircons from eclogite sample HYH01-3 are short prismatic and irregular in shape, with 50–150 μm in length. CL images reveal that most zircon grains are oscillatory-zoned, but the oscillatory bands have commonly been thickened and somewhat blurred (Fig. 2a,b). This feature reflects a magmatic origin of the zircons, which have undergone a post-magmatic solid-state recrystallization (Hoskin and Black, 2000). In addition, two zircon grains show grey homogeneous or cloudy-zoned pattern (Fig. 2c). Twenty-two spot analyses on 14 zircon grains were performed on this sample. The age data are highly scattered, but they can be grouped into three major populations (Fig. 3a). Two homogeneous or cloudy-zoned grains (Nos. 7 and 13) have low Th contents (38–40 ppm) and Th/U ratios (only 0.05–0.06). They yield two Paleoproterozoic $^{207}Pb/^{206}Pb$ ages of 1835±9 and 1865±14 Ma. Among the oscillatory-zoned zircons, four grains (Nos. 4, 6, 11 and 12) have higher Th/U ratios of 0.76 to 1.93 and give a range of $^{206}Pb/^{238}U$ ages from 768±16 Ma to 641±12 Ma. Two other grains (Nos. 8 and 9) yield slightly younger $^{206}Pb/^{238}U$ ages of 541±11 to 424±9 Ma. The remaining six grains show variable Th/U ratios from 0.11 to 1.11 and yield $^{206}Pb/^{238}U$ ages ranging from 250±5 to 193±4 Ma; four of them (Nos. 2, 5, 14 and 15) tightly clustered yielding a weighted mean age of 215±3 Ma ($n=8$, MSWD=1.5). Based on internal structures and Th/U ratios of zircons, two Paleoproterozoic zircon grains must be of metamorphic origin (e.g. Williams and Claesson, 1987; Gebauer et al., 1997; Rubatto and Gebauer, 2000). This suggests that the Paleoproterozoic metamorphic rocks were incorporated in the formation of the protolith of eclogite. The scattered ages of oscillatory-zoned zircons probably reflect different degrees of Pb loss during the late metamorphism. Therefore, we consider the oldest age of 768±16 Ma as the minimum age for the eclogite protolith, whereas the younger concordant age of 215±3 Ma as the recrystallization age of magmatic zircon.

4.1.2. Sample GM02-1: retrograde eclogite from the northern eclogite zone

Zircons from retrograde eclogite sample GM02-1 are prismatic and irregular in shape, with grain sizes varying from 40 to 160 μm. All zircon grains show well-developed fir-tree zoning in the CL images, with or without an irregular, patchy core (Fig. 2d–f). Garnet, omphacite, amphibole, paragonite, epidote, quartz and rutile were observed as inclusions in the fir-tree-zoned domains of the zircon. Thirteen spot analyses were performed on the fir-tree-zoned domains of 9 zircon grains. All such zircon domains, except for spot 7.1 (U=171 ppm, Th=53 ppm, Th/U=0.32), have very low abundances of U (2–50 ppm) and Th (0.01–3.7 ppm), with low Th/U ratios of 0.01 to 0.23. As a consequence, only $^{206}Pb/^{238}U$ ratios are available for most analyses after common Pb correction by assuming that $^{206}Pb/^{238}U$ and $^{208}Pb/^{232}Th$ ages are concordant. Among 13 analyses, in spite of spot 5.1 with a slightly old age (276±14 Ma) and spot 3.2 with a large uncertainty, others yielded two groups of $^{206}Pb/^{238}U$ ages, with one at 255±6 Ma ($n=8$, MSWD=0.17) and another at 216±14 Ma ($n=3$, MSWD=0.034) (Fig. 3b). Taking into account the internal structures and inclusion types in zircons, we interpret the former as the age of eclogite facies metamorphism, and the later as the time of recrystallization of the zircon.

4.1.3. Sample SHZ08-1: eclogite from the southern eclogite zone

Zircons from this sample are mostly irregular in shape, with grain sizes ranging between 30 and 100 μm. All these grains have reworked patchy pattern, with a thin (<5 μm) bright luminescent rim (Fig. 2g). Relict banded zoning is preserved in a few grains. Two other zircon grains are prismatic and show oscillatory zonation, with or without a bright luminescent overgrowth rim (Fig. 2h,i). Eighteen spot analyses on 16 zircon grains were performed. Fourteen patchy grains, except for grain Nos. 9 and 15, plot on or near a discordia with an upper intercept age of 1645±15 Ma and a lower intercept age of 257±16 Ma (MSWD=1.5) (Fig. 3c). One

oscillatory-zoned grain (No. 2) is concordant, giving a $^{206}Pb/^{238}U$ age of 742±11 Ma. Another oscillatory-zoned grain (No. 1) has Th/U ratios ranging from 0.65 to 0.88 and yields young $^{206}Pb/^{238}U$ ages of 256±3 to 240±4 Ma. The upper intercept age of 1645±15 Ma for patchy zircon grains are interpreted to represent the inherited age, whereas the lower intercept age of 257±16 Ma to represent the recrystallization age. The concordant age of 742±11 Ma obtained for Zircon grain No. 2 is comparable with the emplacement age of the eclogite protolith as revealed by sample HYH01-3. Zircon grain No. 1 has a relatively thick (5–15 μm) overgrowth rim, its core domain may have experienced solid-state recrystallization. This zircon grain yielded a comparable age to the lower intercept age of the patchy zircons, and is therefore interpreted to date the eclogite facies metamorphic event.

4.1.4. Sample DFS03-1: metagabbro from the southern eclogite zone

Zircons from metagabbro sample DFS03-1 are irregular in shape, with grain sizes of 50–150 μm. All zircon grains exhibit weak oscillatory

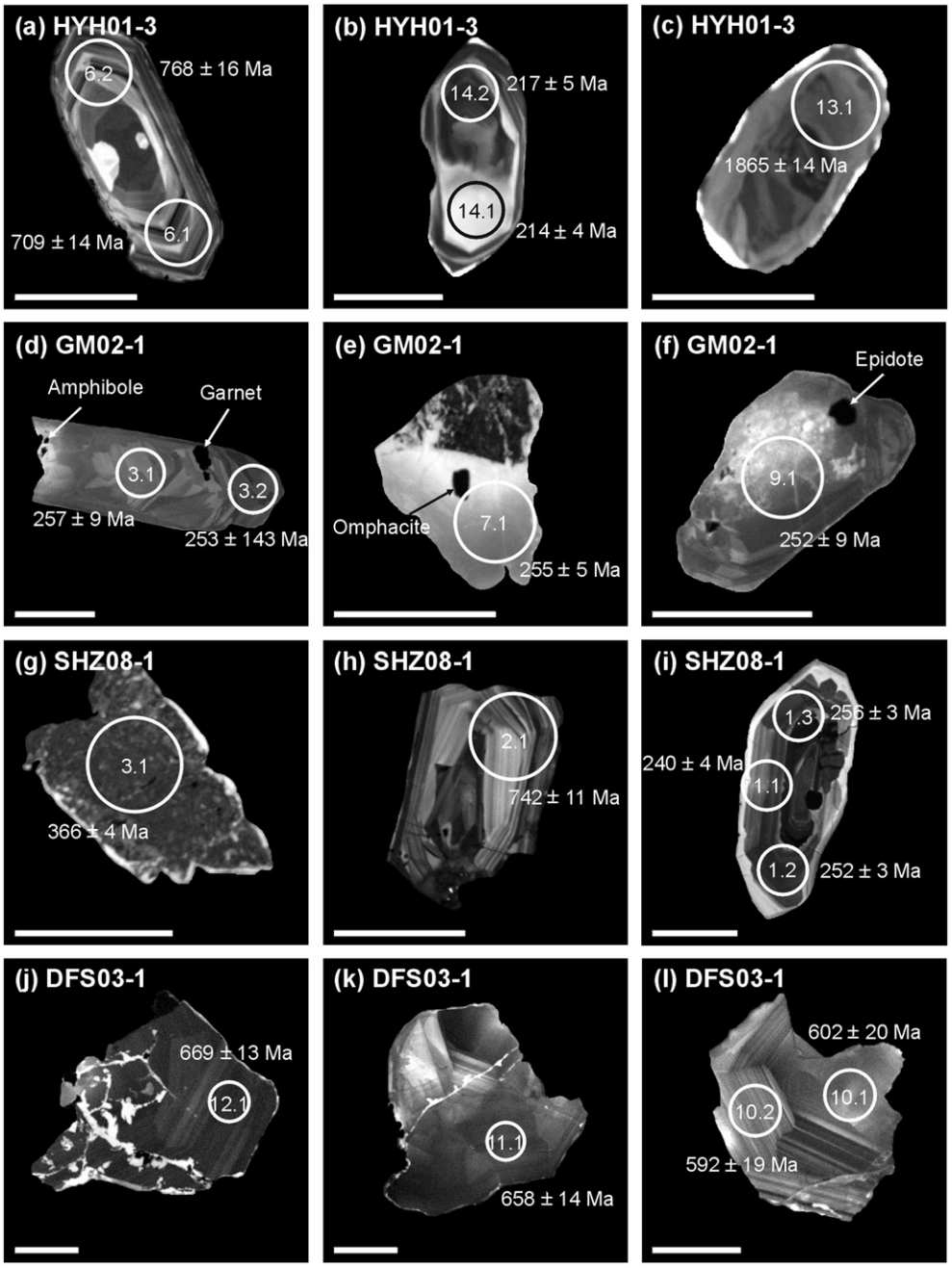

Fig. 2. Representative cathodoluminescence (CL) images of zircons from eclogites (samples HYH01-3, GM02-1 and SHZ08-1) and metagabbro (sample DFS03-1) in the Tongbaishan area. (a) Zircon from sample HYH01-3 showing oscillatory zonation. (b) Zircon from sample HYH01-3 showing oscillatory zonation. The oscillatory bands have been thickened and somewhat blurred, reflecting a post-magmatic solid-state recrystallization. (c) Zircon from sample HYH01-3 showing grey cloudy-zoned pattern. (d) Zircon from sample GM02-1 showing typical fir-tree zoning and containing garnet and amphibole inclusions. (e) Zircon from sample GM02-1 showing fir-tree zoning and containing omphacite inclusion. (f) Zircon from sample GM02-1 showing fir-tree zoning and containing epidote inclusion. (g) Zircon from sample SHZ08-1 showing patchy pattern with a discontinuous bright luminescent rim. (h) Zircon from sample SHZ08-1 showing oscillatory zonation. (i) Zircon from sample SHZ08-1 showing an oscillatory zonation with a bright luminescent rim. (j) Zircon from sample DFS03-1 showing weak oscillatory zonation with several irregular fractures, suggesting a reworking probably by fluid flow. (k) Zircon from sample DFS03-1 showing weak oscillatory zonation with an irregular fracture. (l) Zircon from sample DFS03-1 showing oscillatory zonation. Circles with numbers are SHRIMP analytical spots with their identification numbers. Ages are given at 1σ (see Table 2). Scale bars are 50 μm.

zonation. Some of them develop irregular fractures that were filled by a bright luminescent component, suggesting a recrystallization by fluid flow (Fig. 2j–l). Fifteen U–Pb analyses on 14 zircons yielded two $^{206}Pb/^{238}U$ age populations with one at 662±10 Ma (n=8, MSWD=0.83) and another at 594±13 Ma (n=6, MSWD=0.31) (Fig. 3d). There is no clear difference in both CL images and Th/U ratios (0.28–2.74) between zircons of the two populations. We tentatively interpret the former as the emplacement age of the gabbro, and the later as the time of partial recrystallization probably triggered by fluid flow.

4.1.5. Sample HYH01-11: quartzofeldspathic orthogneiss from the northern eclogite zone

Zircons from quartzofeldspathic orthogneiss sample HYH01-11 are euhedral and short prismatic in shape, with 70–150 μm in length and length to width ratios of about 1.5. Their CL images show strong oscillatory zonation, but many grains have a reworked patchy core (Fig. 4a–c). Except some with a very narrow (<8 μm) bright luminescent rim, no clear metamorphic overgrowth was observed. Twenty-seven spot analyses on 25 zircons were carried out on this sample. Of them twelve analyses plot on or near the Concordia (Fig. 5a), yielding $^{206}Pb/^{238}U$ ages ranging from 763±17 to 708±14 Ma, with a weighted mean of 735±9 Ma (MSWD=1.1) and Th/U ratios of 0.66–1.97. Two other spots (5.1 and 18.1) with older $^{206}Pb/^{238}U$ ages of 799±16 and 777±16 Ma are reversely concordant; their $^{207}Pb/^{206}Pb$ ages are only 686±60 and 700±24 Ma, respectively. The remaining thirteen analyses, including all spots on the patchy domains, tend to lie on the right of the concordia and most show a clear Pb loss. The concordant age of 735±9 Ma is interpreted as the protolith emplacement age of the orthogneiss. The other scattered ages are taken to reflect an influence of both earlier inheritance and later recrystallization.

4.1.6. Sample TB02-1: pelitic schist from the northern eclogite zone

Zircons from this sample are rounded or irregular in shape, with grain sizes varying from 50 to 120 μm. Most zircon grains show grey planar and/or sector zoning with a narrow or thick bright luminescent rim. Some have a small oscillatory-zoned relict core (Fig. 4d–f). Of fifteen U–Pb analyses on 11 zircon grains (Fig. 5b), two spots (4.1 and 8.1) on oscillatory-zoned core yield old $^{207}Pb/^{206}Pb$ ages of 1936±9 Ma (Th/U=0.12) and 1882±10 Ma (Th/U=0.38). The age of 1936±9 Ma is very similar to that obtained for zircons from sample DFS06-1 (see below). The other thirteen spots yield $^{207}Pb/^{206}Pb$ age concentrated between 1781±16 and 1884±10 Ma, with Th/U ratios as low as 0.01–0.18. Of them eight analyses are highly clustered, giving a weighted mean age of 1820±6 Ma (SMWD=0.59), which is interpreted as the time of metamorphism.

4.1.7. Sample DFS06-1: quartzite from the southern eclogite zone

Zircons from quartzite sample DFS06-1 are rounded or ovoid in shape, with grain sizes ranging from 200 to 400 μm. Based on morphology and CL image, the zircons can be divided into two groups (Fig. 4g–i). Group I zircons are long ovoid and have an oscillatory/sector-zoned core and a thin

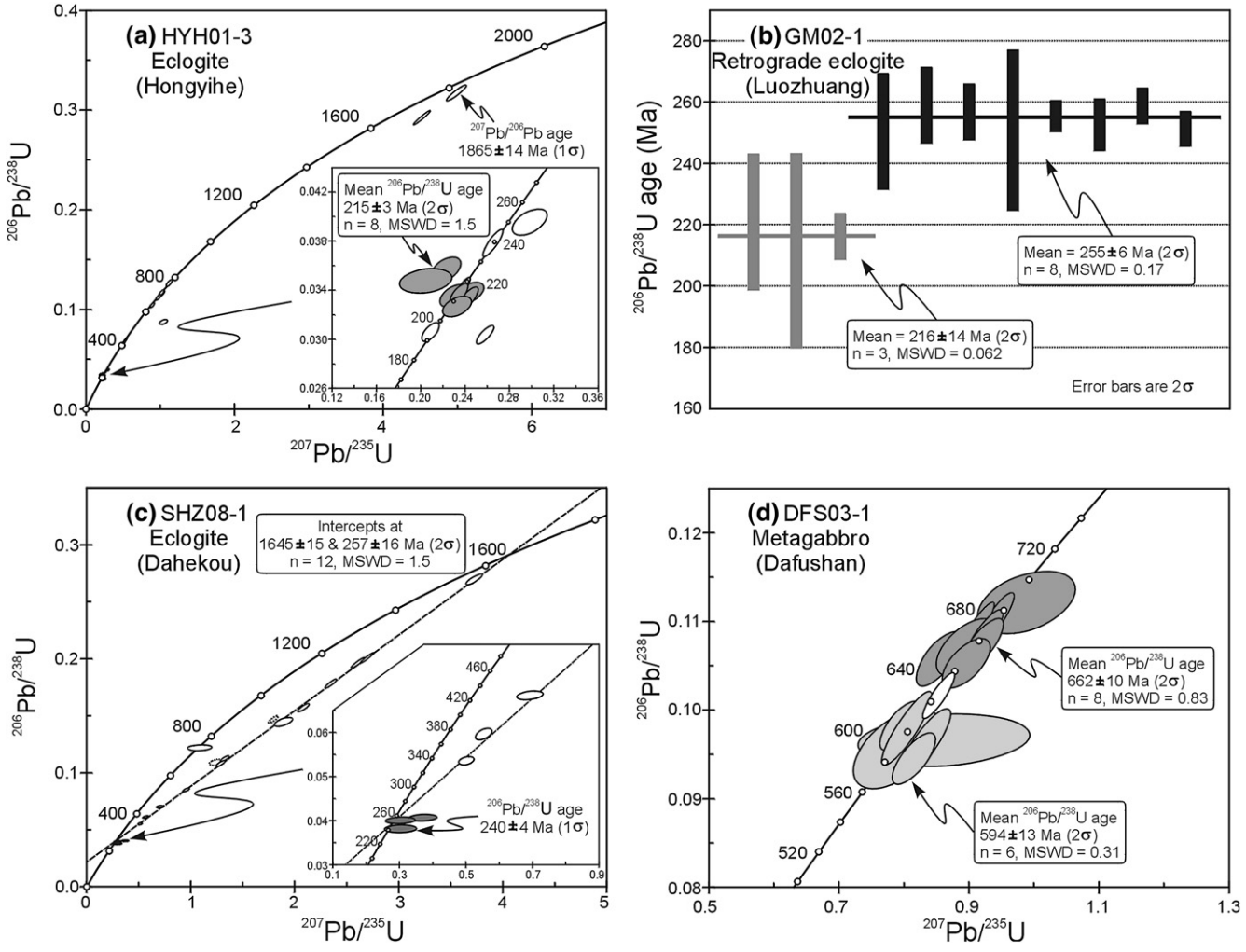

Fig. 3. SHRIMP zircon U–Pb concordia diagrams of eclogites (a, sample HYH01-3; c, SHZ08-1) and metagabbro (d, sample DFS03-1) and distribution plots of $^{206}Pb/^{238}U$ ages of retrograde eclogite (b, sample GM02-1) from the Tongbaishan area.

homogeneous grey rim. SHRIMP analyses reveal that two such zircon cores yield $^{207}Pb/^{206}Pb$ ages are 2541±16 Ma (Th/U=2.93) and 2519±9 Ma (Th/U=0.38), respectively, whereas overgrowth rims yield $^{207}Pb/^{206}Pb$ ages ranging from 2509±9 to 2460±24 Ma, with a mean of 2490±11 Ma (n=5, MSWD=0.81) and Th/U ratios of 0.15–0.68 (Fig. 5c). Group II zircons are mostly rounded and show oscillatory and sector zonation but one grain is prismatic and contains a rounded oscillatory-zoned core (see Fig. 4g). The data on such zircon core (spot 9.1) gives a slightly old $^{207}Pb/^{206}Pb$ age of 2348±17 Ma. All other analyses on oscillatory/sector-zoned domains yield $^{207}Pb/^{206}Pb$ ages ranging from 2072±25 to 1862±41 Ma, with Th/U ratios of 0.39–1.21. Of them eleven analyses form a discordant array with an upper intercept age of 1934±8 Ma, which is identical within error with the weighted mean age of 1930±7 Ma (MSWD=1.5) obtained for the same analyses. The core age of 2541±16 Ma and rim age of 2490±11 Ma for

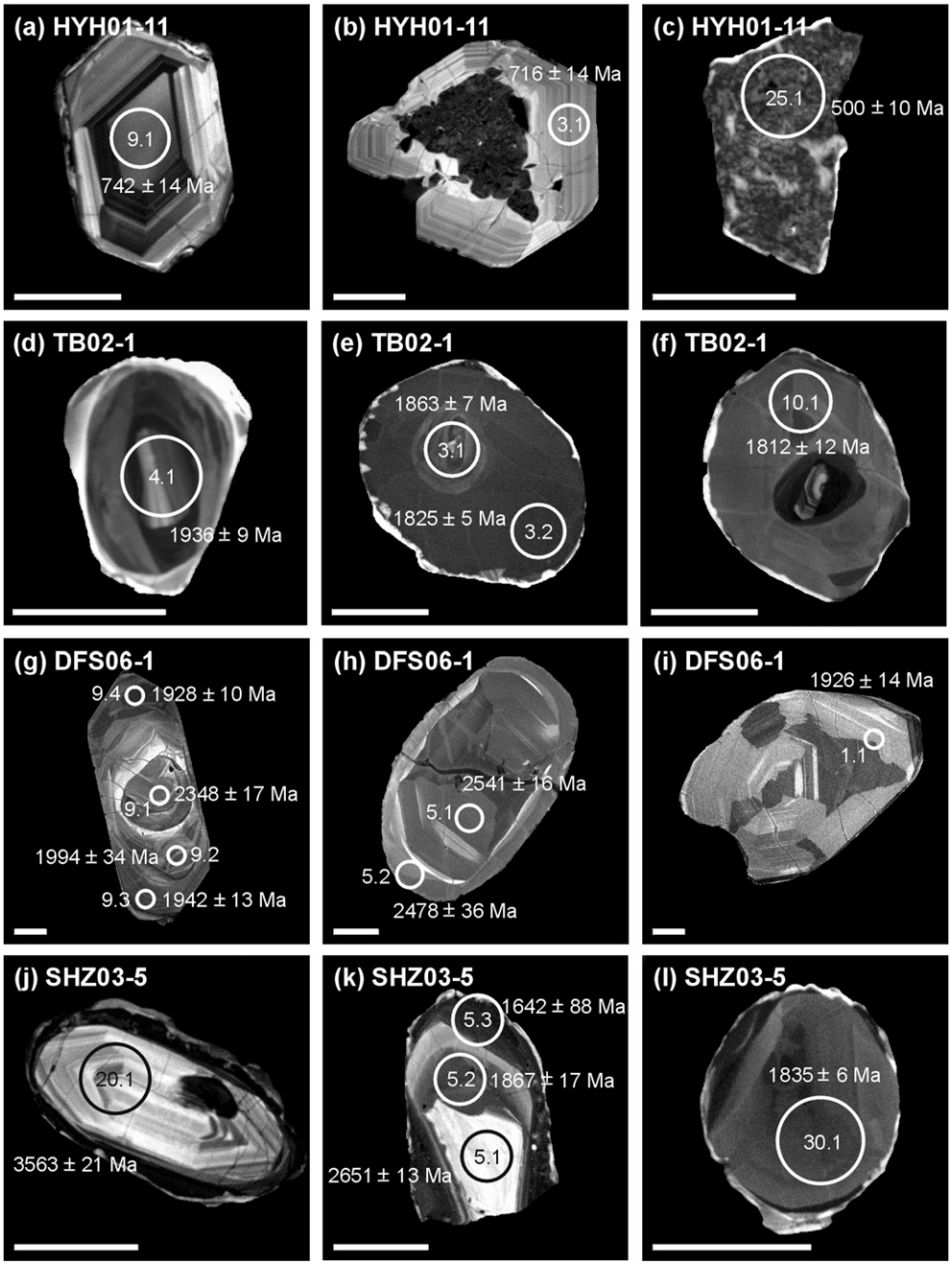

Fig. 4. Representative cathodoluminescence (CL) images of zircons from quartzofeldspathic orthogneiss (sample HYH01-11), pelitic schist (sample TB02-1), quartzite (sample DFS06-1) and quartzofeldspathic paragneiss (sample SHZ03-5) in the Tongbaishan area. (a) Zircon from sample HYH01-11 showing oscillatory zonation. (b) Zircon from sample HYH01-11 showing a patchy core and an oscillatory-zoned rim. (c) Zircon from sample HYH01-11 showing patchy pattern. (d) Zircon from sample TB02-1 showing an oscillatory-zoned core, a planar-zoned mantle and a bright luminescent rim. (e) Zircon from sample TB02-1 showing planer/sector zonation with an oscillatory-zoned relict core and a discontinuous bright luminescent rim. (f) Zircon from sample TB02-1 showing planer/sector zonation with an oscillatory-zoned relict core and a discontinuous bright luminescent rim. (g) Zircon from sample DFS06-1 showing a rounded oscillatory-zoned core and an oscillatory/sector-zoned rim. (h) Zircon from sample DFS06-1 showing an oscillatory/sector-zoned core and a homogeneous grey rim. (i) Zircon from sample DFS06-1 showing oscillatory and sector zonation. (j) Zircon from sample SHZ03-5 showing an oscillatory-zoned core and an irregular dark/grey luminescent rim. (k) Zircon from sample SHZ03-5 showing a bright oscillatory-zoned core, a grey planar-zoned mantle and a dark planar-zoned rim. Zircon grain has a thin and discontinuous bright luminescent rim, probably reflecting a late growth. (l) Zircon from sample SHZ03-5 showing a dark planar/sector zonation with a discontinuous bright luminescent rim. Circles with numbers are SHRIMP analytical spots with their identification numbers. Ages are given at 1σ (see Table 2). Scale bars are 50 μm.

Group I zircons are taken to be igneous and metamorphic ages, respectively, while the age of 1930±7 Ma is interpreted to represent the timing of another igneous event occurring in the area.

4.1.8. Sample SHZ03-5: quartzofeldspathic paragneiss from the southern eclogite zone

Zircons from this sample are also rounded or ovoid in shape, with grain sizes ranging from 50 to 200 μm. CL images reveal that most zircon grains have an oscillatory-zoned core and a dark or grey planar/sector-zone rim, but some zircon cores also show grey planar/sector zonation. Furthermore, almost all the zircon grains have a very thin (<5 μm), bright luminescent rim (Fig. 4j–l), probably reflecting a late growth. Thirty-four U–Pb analyses on 30 zircons reveal a very complex age pattern (Fig. 5d). For the oscillatory-zoned zircon domains, one spot analyses (20.1) produces an oldest $^{207}Pb/^{206}Pb$ age of 3563±21 Ma, with a Th/U ratio of 0.74; others yield $^{207}Pb/^{206}Pb$ ages scattered from 2730±42 to 2002±130 Ma, with Th/U ratios ranging from 0.17 to 1.11. All these zircon domains are of magmatic origin. For the planar/sector-zoned zircon domains, $^{207}Pb/^{206}Pb$ ages obtained are scattered from 1880±6 to 1391±21 Ma. Their Th/U ratios range from 0.06 to 0.38. Among them, nine analyses define a discordant array with an upper intercept age of 1851±9 Ma, which is in agreement within error with the weighted mean age of 1846±5 Ma (MSWD=1.9) obtained for the same analyses. Taking into account the CL features and low Th/U ratios for such zircon domains, this age is interpreted to represent the timing of a metamorphic event occurring in the area. Note that most zircon domains show the different degrees of Pb loss due to the effect of Phanerozoic thermal event, which is likely in response to the HP metamorphism.

4.2. $^{40}Ar/^{39}Ar$ muscovite ages

Muscovites of the five dated samples are all fine-grained, idiomorphic, and strongly oriented to form foliation of the rocks (Fig. 6a–e). The flakes of muscovite generally have a width of 0.1–0.3 mm and a length of 0.5–1.0 mm, but those of sample DFS06-1 are smaller. Some muscovite crystals contain inclusions of plagioclase, K-feldspar, quartz and ilmenite. Small amount of paragonite occurs as intergrowth with muscovite in sample SHZ03-5 (Fig. 6f).

Electron microprobe analysis of muscovite showed variable Si contents (3.11–3.43 per formula unit) and Mg/(Fe+Mg) (0.11–0.69) and Na/(Na+K) ratios (0.004–0.147) between samples (Fig. 7), suggesting that muscovites from some samples have been subjected to retrograde reactions and/or chemical modifications during the exhumation of the HP rocks. However, within a single thin section, the compositional variation of muscovite crystals is very limited. Note that the muscovite compositions in sample GJZ10-1 plot far beneath the ideal Tschermak substitution line in Si–Al diagram due to a substantial Ai–Fe^{3+} substitution.

Among five dated samples, four samples yield Triassic plateau ages of 238±2 (HYH01-11), 238±2 (GM02-4), 217±1 (GJZ10-1) and 234±2 Ma (DFS06-1) over more than 83% of the ^{39}Ar released (Fig. 8a,c,e,g). Inverse

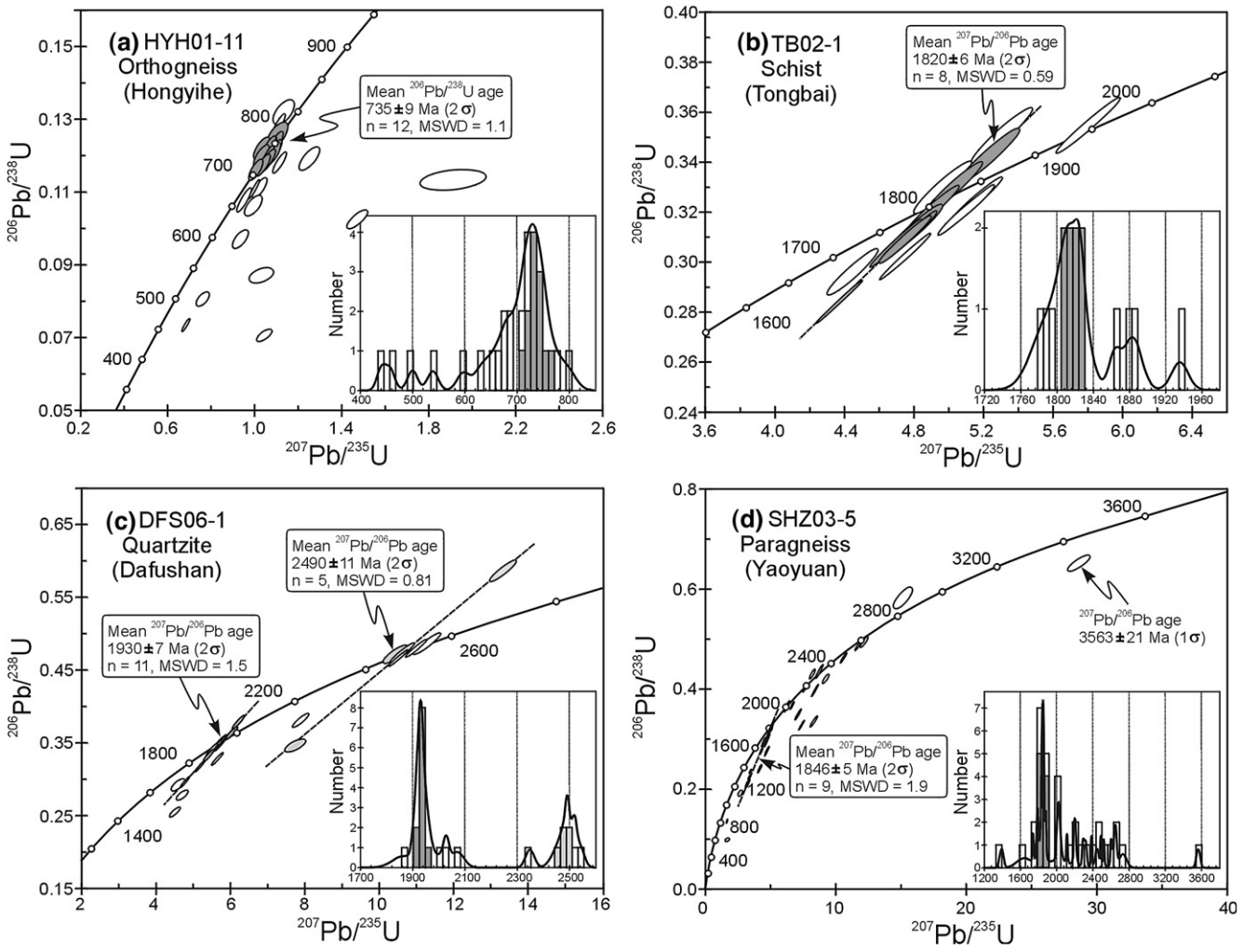

Fig. 5. SHRIMP zircon U–Pb concordia diagrams of quartzofeldspathic orthogneiss (a, sample HYH01-11), pelitic schist (b, sample TB02-1), feldspathic quartzite (c, sample DFS06-1) and quartzofeldspathic paragneiss (d, sample SHZ03-5) from the Tongbaishan area.

isochron plots yield ages within error of the plateau ages (Fig. 8b,d,f,h). Another sample (SHZ03-5) displays an old, Carboniferous plateau age of 337±2 Ma over almost 100% of the ^{39}Ar released (Fig. 8i). Inverse isochron age is 334±4 Ma (Fig. 8j), identical within error with plateau age. The muscovite plateau age is commonly inferred to reflect the time of cooling of the muscovite through its closure temperature of ca. 350 °C (Hames and Bowring, 1994).

5. Discussion

5.1. Age and provenance of protoliths

For the Qinling–Dabie–Sulu orogen, the ages of inherited zircons can be used to determine the provenance of the Sino-Korean or Yangtze craton and therefore the location of the suture (Hacker et al., 1998, 2006). As generally accepted, the distinctive ca. 750 Ma bimodal magmatism are diagnostic of the Yangtze craton (Hacker et al., 1998, 2000) and its occurrence was related to the rifting of the supercontinent Rodinia (Li et al., 2003). Four Neoproterozoic protolith ages of 768±16 Ma, 742±11 Ma, 733±7 Ma and 662±10 Ma were obtained for eclogite, metagabbro and orthogneiss from the Tongbaishan area. These data are consistent with U–Pb zircon ages reported for various lithologies from eastern and western Dabieshan (e.g. Ames et al., 1993, 1996; Rowley et al., 1997; Xue et al., 1997; Hacker et al., 1998, 2000; Liu et al., 2003, 2004a; Zheng et al., 2004, 2006), and therefore demonstrates that the Tongbaishan HP rocks is a coherent part of the Dabie HP/UHP terrane.

U–Pb dating on detrital zircons from sedimentary rocks is commonly used to trace depositional ages, material sources and the earlier crustal histories of geological terranes. Three major age

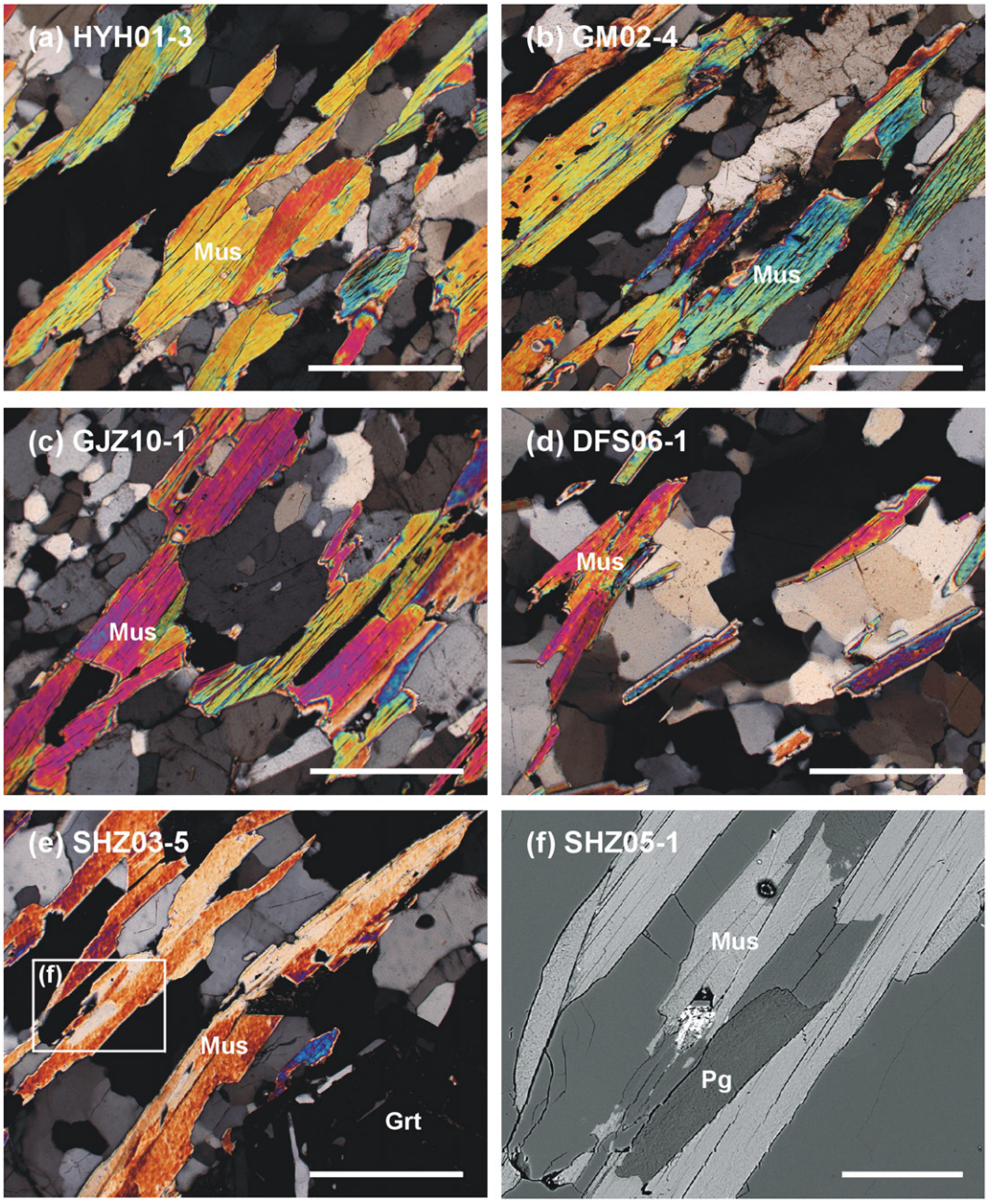

Fig. 6. Photomicrographs (a–e) and backscattered electron image (f) showing the mode of occurrence of white mica in thin sections. Scale bars are 0.5 mm for (a)–(e), and 0.1 mm for (f). Mineral abbreviations: Grt = garnet; Mus = muscovite; Pg = paragonite.

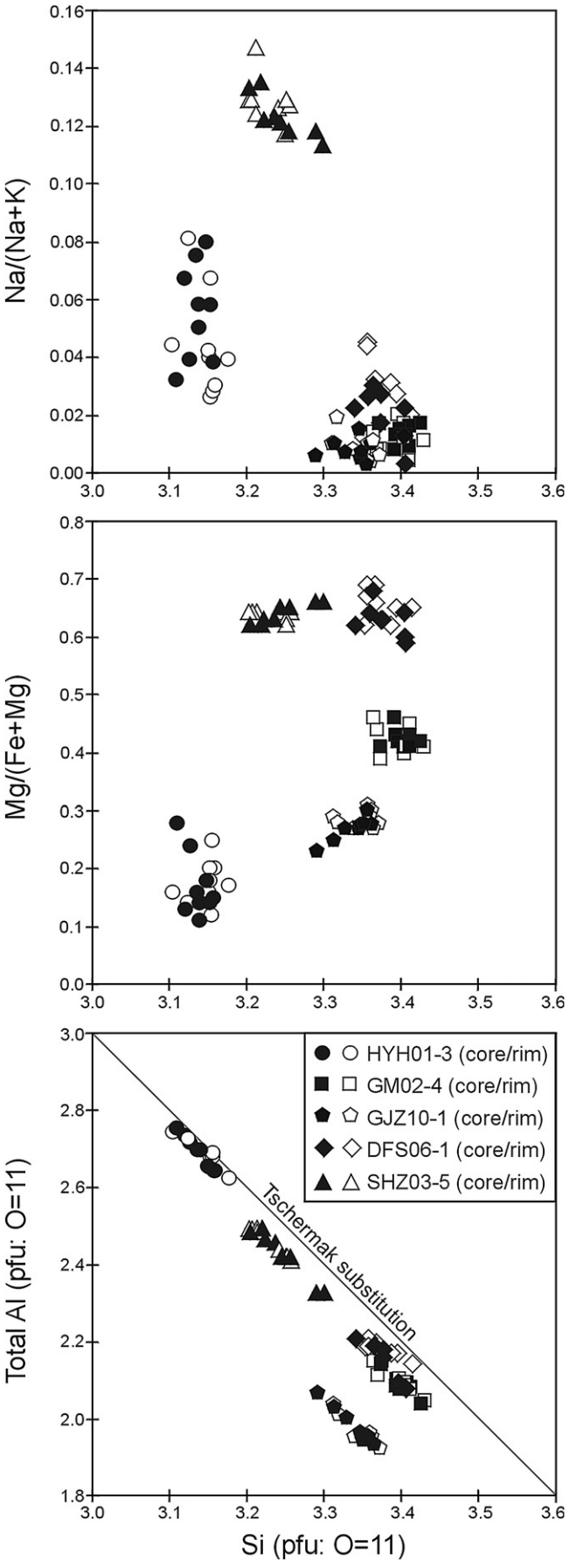

Fig. 7. Chemical variation diagrams [(Si–Al, Si–Mg/(Fe+Mg) and Si–Na/(Na+K)] of muscovite in thin sections.

populations of 2.49 Ga, 1.93 Ga and 1.85–1.82 Ga and an age as old as 3.56 Ga (Fig. 9) were obtained for detrital zircons from metasedimentary rocks in the Tongbaishan area. Textures observed by CL imaging indicate that the oldest detrital zircon grain of 3.56 Ga is of magmatic origin. This is the second occurrence of >3.5 Ga zircon grains (first one from Chen et al., 2003a) reported from the Dabie orogen. Other age populations of 2.49 Ga, 1.93 Ga and 1.85–1.82 Ga indicate three major tectonothermal events occurring in the source region of these rocks. No ca. 750 Ma detrital zircon grains were identified from all three dated paragneisses, suggesting that the deposition of the materials probably took place prior to the middle Neoproterozoic time.

The age patterns, particularly age populations of 1.93 Ga and 1.85–1.82 Ga, are very similar to those obtained from the Trans-North China Orogen, north of the Tongbaishan area (Zhao et al., 2004). This seems to imply the Sino-Korean craton as a possible source of the Tongbaishan paragneisses, as suggested by Chen et al. (2003a) for the Foziling Group of eastern Dabieshan. However, similar zircon ages have also been reported for various rocks including eclogites, quartzites, marbles and granites from the Dabie–Sulu orogen (Ayers et al., 2002; Chen et al., 2003a,b, Yang et al., 2003b; Bryant et al., 2004; Li et al., 2004; Tang et al., 2004; Hacker et al., 2006; Liu et al., 2006a; Wu et al., 2006). Furthermore, the Paleoproterozoic metamorphic event of ca. 1.95 Ga was recently identified in metamorphic rocks from the Archaean Kongling terrane and the surrounding Neoproterozoic sedimentary rocks (Qiu et al., 2000; Ling et al., 2001; Zhang et al., 2006a,b). This suggests that the northern margin of the Yangtze craton may have involved an extensive Paleoproterozoic orogenesis.

5.2. Timing of metamorphism

SHRIMP U–Pb analysis of zircon is a powerful technique to trace the tectonothermal history of multiple metamorphic terranes. Application of such technique to rocks metamorphosed at lower temperatures (<600 °C) has been scanty and it remains largely unexplored though zircon can grow at these conditions in the presence of hydrous fluids (Rubatto et al., 1998, 1999; Liermann et al., 2002). In the low-temperature HP rocks from the Tongbaishan area, except for those from retrograde eclogite sample GM02-1, most zircons grains from other eclogites and gneisses only have a very narrow (mostly less than 8 μm) overgrowth rim, or even do not show growth under eclogite facies conditions. Some zircons, particularly those from eclogites, have experienced different degrees of solid-state recrystallization, as shown by blurred oscillatory bands or reworked patchy pattern in the CL images. A $^{206}Pb/^{238}U$ age of 255±6 Ma was obtained for HP-phase-bearing zircon domains from sample GM02-1, and a lower intercept age of 257±16 Ma was obtained for patchy zircon grains from sample SHZ08-1. These ages are in agreement with the phengite-based (phengite–amphibole–omphacite–garnet–whole rock) Rb–Sr isochron age of 253±11 Ma (initial $^{87}Sr/^{86}Sr = 0.72174 \pm 0.00010$) obtained for eclogite sample SHZ04-2 (Table 5, Fig. 10), 1.5 km east of sample SHZ03-5 (32°23′09″ N, 112°52′58″ E). This indicates that HP eclogite facies metamorphism in the Tongbaishan area took place at ca. 255 Ma. In addition, the concordant age of ca. 215 Ma obtained for samples HYH01-3 and GM02-1 may suggest a later phase of zircon recrystallization.

$^{40}Ar/^{39}Ar$ muscovite dating could also provide important constraints on the timing of low-temperature HP metamorphism. The flat age spectra of muscovite for all samples seem to suggest that $^{40}Ar/^{39}Ar$ ages obtained herein are not affected by excess Ar (e.g. Hacker et al., 2000). Two samples (HYH01-11 and GM02-4) with oldest $^{40}Ar/^{39}Ar$ ages of 238±2 Ma come from the northern eclogite zone (i.e. Huwan HP unit). These ages are probably within error with two ages of 235±2 Ma and 235±3 Ma reported for the same unit in western Dabieshan (Webb et al., 1999; Ratschbacher et al., 2006). Another sample (DFS06-1) with age of 234±2 Ma come from the southern eclogite zone (i.e. Hong'an HP unit). This age is also

comparable with the older age group of 237±2 Ma to 231±2 Ma from the same unit in western Dabieshan (Eide et al., 1994; Webb et al., 1999). Sample GJZ10-1 was collected about 50 km southwest of the Xiongdian eclogite from the northwestern corner of western Dabieshan. Its $^{40}Ar/^{39}Ar$ muscovite age of 217±1 Ma is identical within error to the U–Pb zircon recrystallization age of 215±3 Ma obtained for the Hongyihe eclogite (sample HYH01-3). Many similar ages of ca. 218–210 Ma are also reported for the different units of western Dabieshan (Eide et al., 1994; Webb et al., 1999, 2001; Liu et al., 2004a; Jahn et al., 2005; Ratschbacher et al., 2006). Therefore, westward extension of the Dabieshan HP/UHP terrane to the Tongbaishan area is further documented by the similarity of metamorphic ages between the two areas.

The $^{40}Ar/^{39}Ar$ muscovite age of 337±2 Ma obtained for a quartzofeldspathic paragneiss (sample SHZ03-5) from the southern eclogite zone is enigmatic. This age seems to be comparable with the metamorphic age of 309±3 Ma obtained by SHRIMP U–Pb zircon dating for the Xiongdian eclogite from western Dabieshan (Sun et al., 2002). A similar metamorphic event of 316–304 Ma was also reported from amphibolites in the southern margin of the Qinling arc (Zhai et al., 1998). However, these two localities are within or outside the northern margin of the Triassic HP/UHP terrane, which could be explained by the Carboniferous accretionary orogenesis prior to the Triassic collision between the Sino-Korean and Yangtze cratons. In the south of the UHP unit in the Dabieshan and Sulu areas, however, the effect of the Carboniferous HP metamorphism has never been evidenced.

The chemical compositions of muscovites from sample SHZ03-5 are characterized by high Na/(Na+K) ratios. It has been shown that muscovite (phengite) with high Na/(Na+K) ratios from eclogites commonly yielded anomalously old $^{40}Ar/^{39}Ar$ ages (Boundy et al., 1997; Chen et al., 2007). Consequently, the $^{40}Ar/^{39}Ar$ plateau age of 337±2 Ma for the paragneiss was probably produced by excess Ar, although the age spectrum of muscovite from this sample is rather flat and almost includes 100% of the ^{39}Ar released. The same situation of excess Ar with 100% plateau was demonstrated in phengite of a mica schist from a UHP metamorphic terrane of Mali (Jahn et al., 2001). The Mali eclogites and mica schists recorded the oldest UHP metamorphic event of the world at ca. 620 Ma, but the phengite $^{40}Ar/^{39}Ar$ age is 1045±9 Ma. Alternatively, because of the mixing of minor paragonite with muscovite, the step-heated analyses may show an artifact (Boundy et al., 1997), as the case for biotite/chlorite (Lo and Onstott, 1989). In any case, this age does not seem to reflect meaningful geological event.

5.3. Implications for exhumation of the HP/UHP rocks

Three groups of Triassic ages (ca. 255 Ma, ca. 238 Ma and ca. 215 Ma) were obtained for rocks from the Tongbaishan area using the zircon U–Pb and muscovite $^{40}Ar/^{39}Ar$ dating techniques. The presence of HP mineral inclusions and the development of fir-tree structure in zircons indicate that the age of ca. 255 Ma most probably represents the time of eclogite facies metamorphism as a result of continental subduction. The age of ca. 238 Ma comes from $^{40}Ar/^{39}Ar$ dating on muscovite. We interpret it to reflect the time of exhumation of the HP rocks. The age of ca. 215 Ma corresponds to a $^{40}Ar/^{39}Ar$ phengite age of 215±1 Ma from the Huwan HP unit (Huwan shear zone) of western Dabieshan, where the phengite dated top-to-north flow along phengite-rich shear bands within the retrograded outer margin of a small eclogite body (Ratschbacher et al., 2006). Thus, this age group is related to the later phase of deformation and recrystallization of the HP rocks.

In recent years, precise dating using the SHRIMP technique on different domains of zircon from UHP rocks of the Dabieshan and Sulu terranes has also revealed three Triassic age groups at ca. 240 Ma, ca. 227 Ma and ca. 216 Ma (Li et al., 2004; Wan et al., 2005; Hacker et al., 2006; Leech et al., 2006; Liu et al., 2006a,b; Wu et al., 2006, 2008). The three age groups were considered by some workers to reflect different stages of metamorphic evolution from prograde through peak to retrograde episodes. Such consideration was based on internal structures of zircons and their mineral inclusions, as well as rare-earth element patterns and Hf and O isotopic compositions of zircons (Li et al., 2004; Liu et al., 2006a,b; Wu et al., 2006). However, some others argued that the first age group might also record the UHP metamorphic episode (Wan et al., 2005; Hacker et al., 2006). In comparison, the oldest $^{40}Ar/^{39}Ar$ muscovite ages are clustered at about 213 Ma for the Sulu UHP terrane (Webb et al., 2006), and ≤216 Ma for the Dabieshan UHP terrane (Eide et al., 1994; Webb et al., 1999, 2001; Hacker et al., 2000). In any case, the above age data provide a temporal framework for the geodynamic process from deep subduction to exhumation of the UHP continental slice.

The different age patterns between the HP and UHP rocks from the Tongbaishan, Dabieshan, and Sulu areas suggest that, when a crustal slice was subducted to mantle depths and underwent UHP metamorphism, the slice overlain it, probably represented by the Huwan and Hong'an HP units, might have been exhumed to mid- to upper-crustal levels and cooled to below ca. 350 °C. The exhumation of the UHP slice could postdate the HP slice by about 25 Ma. In fact, Liu et al. (2004a,b) proposed a similar scenario in which successive subduction and exhumation of the broken slices of the subducting Yangtze slab took place in the Triassic. Any later deformation associated with further exhumation of the UHP slice might have partially affected the HP slice, thus resulted in two groups of cooling ages recorded in the HP rocks. The absence of UHP rocks in the Tongbaishan area may reflect a shallower subduction or a smaller extent of exhumation towards the west of the Dabie–Sulu terrane (Hacker et al., 2000; Ernst et al., 2007).

6. Conclusions

(1) U–Pb zircon analyses of eclogite, metagabbro and orthogneiss from the Tongbaishan area reveal an extensive bimodal magmatism in the period of 768–662 Ma, whereas detrital zircons from metasedimentary rocks reveal three major tectonothermal events of 2.49 Ga, 1.93 Ga and 1.85–1.82 Ga. The new age data suggest that the northern margin of the Yangtze craton involves a Paleoproterozoic orogenesis and a Neoproterozoic rifting.

(2) $^{40}Ar/^{39}Ar$ dating of muscovite from quartzofeldspathic gneiss and quartzite yield two major deformation episodes at 238 and 217 Ma, respectively. These ages, coupled with zircon recrystallization ages of 255 and 215 Ma obtained for eclogites, suggest that the HP rocks from the Tongbaishan area were metamorphosed during the Permian–Triassic period and the area is the westward continuation of the Dabie–Sulu UH/UHP terrane.

(3) The subduction of the HP slice in the Tongbai–Dabie–Sulu orogen commenced at ca. 255 Ma, slightly earlier than the timing of deep subduction of the UHP slice. Furthermore, the diachronous exhumation lasted from ca. 238 Ma for the HP slice to ca. 213 Ma for the UHP slices. This could be explained by successive subduction and exhumation of the broken slices of the subducting Yangtze slab.

Acknowledgements

We would like to thank Ping Jian, Wei Zhang and Biao Song for assistance in the SHRIMP U–Pb zircon analyses and Wen Chen and Yan Zhang in the $^{40}Ar/^{39}Ar$ muscovite analyses. Critical reviews by two anonymous reviewers and editorial comments by I. Buick substantially improved the manuscript. The research of the senior author was supported by the National Natural Science Foundation of China (No. 40672047), Geological Investigation Project of China Geological Survey (1212010711812) and Free Research Project of MLR (2002406). Bor-ming Jahn acknowledges the financial support of the

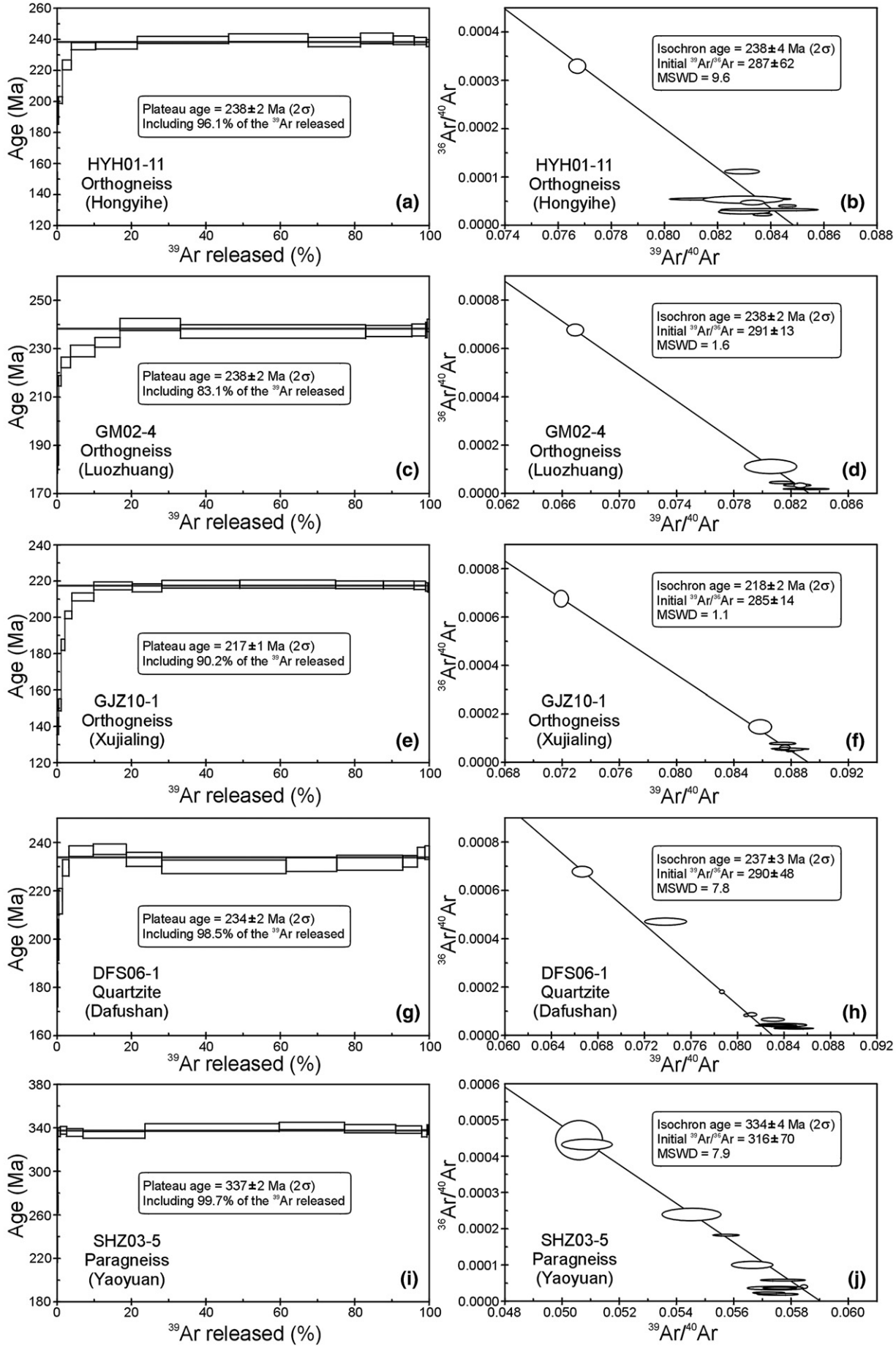
Plateau age = 238±2 Ma (2σ)
Including 96.1% of the 39Ar released
HYH01-11
Orthogneiss
(Hongyihe)
(a)
Isochron age = 238±4 Ma (2σ)
Initial 39Ar/36Ar = 287±62
MSWD = 9.6
HYH01-11
Orthogneiss
(Hongyihe)
(b)
Plateau age = 238±2 Ma (2σ)
Including 83.1% of the 39Ar released
GM02-4
Orthogneiss
(Luozhuang)
(c)
Isochron age = 238±2 Ma (2σ)
Initial 39Ar/36Ar = 291±13
MSWD = 1.6
GM02-4
Orthogneiss
(Luozhuang)
(d)
Plateau age = 217±1 Ma (2σ)
Including 90.2% of the 39Ar released
GJZ10-1
Orthogneiss
(Xujialing)
(e)
Isochron age = 218±2 Ma (2σ)
Initial 39Ar/36Ar = 285±14
MSWD = 1.1
GJZ10-1
Orthogneiss
(Xujialing)
(f)
Plateau age = 234±2 Ma (2σ)
Including 98.5% of the 39Ar released
DFS06-1
Quartzite
(Dafushan)
(g)
Isochron age = 237±3 Ma (2σ)
Initial 39Ar/36Ar = 290±48
MSWD = 7.8
DFS06-1
Quartzite
(Dafushan)
(h)
Plateau age = 337±2 Ma (2σ)
Including 99.7% of the 39Ar released
SHZ03-5
Paragneiss
(Yaoyuan)
(i)
Isochron age = 334±4 Ma (2σ)
Initial 39Ar/36Ar = 316±70
MSWD = 7.9
SHZ03-5
Paragneiss
(Yaoyuan)
(j)
Age (Ma)
39Ar released (%)
36Ar/40Ar
39Ar/40Ar

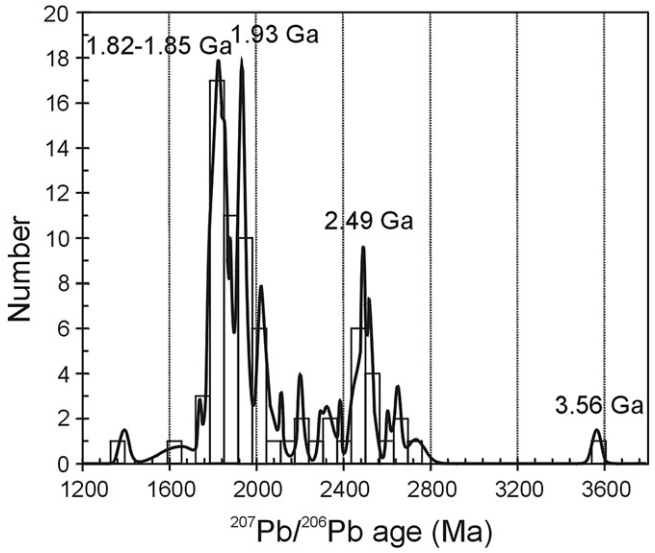

Fig. 9. Plot of cumulative probability histogram for ^{207}Pb/^{206}Pb ages of detrital zircons from metasedimentary rocks in the Tongbaishan area.

NSC of Taiwan (NSC93-2116-M-001-22, NSC94-2116-M-001-08 and NSC 95-2116-M-001-20).

Table 5
Rb–Sr isotopic compositions for the Chengyao eclogite (sample SHZ04-2) from the Tongbaishan area

Whole rock and mineral	Rb (ppm)	Sr (ppm)	^{87}Rb/^{86}Sr	^{87}Sr/^{86}Sr	±2 σm	Isochron age (Ma)	Initial ratio (metamorphic)
WR	6.98	216.3	0.093	0.722112	9	253±11	0.72174±10
Grt	0.37	58.99	0.018	0.721740	8		
Omp	0.82	171.7	0.014	0.721751	6		
Phg	339.7	405.2	2.43	0.730478	10		
Amp	1.53	167.3	0.026	0.721906	7		

Rb–Sr isotope analyses were performed at Géosciences Rennes. Analytical procedures were described by Chavagnac and Jahn (1996). Phengite-based isochron age is calculated using ISOPLOT/Ex 2.01 (Ludwig, 1999). Error input in isochron calculation is 2% for ^{87}Rb/^{86}Sr, and 0.005% for ^{87}Sr/^{86}Sr. Decay constant (λ^{87}Rb) used is 0.0142 Ga^{-1}. Mineral abbreviations are as in Table 1 except for WR = whole rock.

References

Ames, L., Tilton, G.R., Zhou, G., 1993. Timing of collision of the Sino-Korean and Yangtze cratons: U–Pb zircon dating of coesite-bearing eclogites. Geology 21, 339–342.

Ames, L., Zhou, G., Xiong, B., 1996. Geochronology and isotopic character of ultrahigh-pressure metamorphism with implications for collision of the Sino-Korean and Yangtze Cratons, central China. Tectonics 15, 472–489.

Ayers, J.C., Dunkle, S., Gao, S., Miller, C.F., 2002. Constraints on timing of peak and retrograde metamorphism in the Dabie Shan ultrahigh-pressure metamorphic belt, east-central China, using U–Th–Pb dating of zircon and monazite. Chem. Geol. 186, 315–331.

Black, L.P., Kamo, S.L., Allen, C.M., Aleinikoff, J.N., Davis, D.W., Korsch, R.J., Foudoulis, C., 2003. TEMORA 1: a new standard for Phanerozoic U–Pb geochronology. Chem. Geol. 200, 155–170.

Boundy, T.M., Hall, C.M., Li, G., Essene, E.J., Halliday, A.N., 1997. Fine-scale isotopic heterogeneities and fluids in the deep crust: a ^{40}Ar/^{39}Ar laser ablation and TEM study of muscovites from a granulite–eclogite transition zone. Earth Planet. Sci. Lett. 148, 223–242.

Bryant, D.L., Ayers, J.C., Gao, S., Miller, C.F., Zhang, H.F., 2004. Geochemical, age, and isotopic constraints on the location of the Sino-Korean/Yangtze suture and evolution of the Northern Dabie complex, east central China. Geol. Soc. Am. Bull. 116, 698–717.

Chavagnac, V., Jahn, B.-M., 1996. Coesite-bearing eclogites from the Bixiling Complex, Dabie Mountains, China: Sm–Nd ages, geochemical characteristics and tectonic implications. Chem. Geol. 133, 29–51.

Chen, W., Zhang, Y., Ji, Q., Wang, S., Zhang, J., 2002. The magmatism and deformation times of the Xidatan rock series, East Kunlun Mountain. Sci. China (Ser. B) (Supplement), 45, 20–27.

Chen, F.K., Guo, J.H., Jiang, L.L., Siebel, W., Cong, B., Satir, M., 2003a. Provenance of the Beihuaiyang lower-grade metamorphic zone of the Dabie ultrahigh-pressure collisional orogen, China: evidence from zircon ages. J. Asian Earth Sci. 22, 343–352.

Chen, D.G., Etienne, D., Cheng, H., Xia, Q.K., Wu, Y.B., 2003b. Preliminary study of microscale zircon oxygen isotopes for Dabie–Sulu metamorphic rocks: ion probe in situ analyses. Chin. Sci. Bull. 48, 1670–1678.

Chen, W., Zhang, Y., Liu, X.Y., Wang, Q.L., 2007. New achievements in the study of the excess argon in HP–UHP metamorphic minerals. Geochim. Cosmochim. Acta (Supplement) 71, A167.

Ernst, W.G., Tsujimori, T., Zhang, R., Liou, J.G., 2007. Permo-Triassic collision, subduction-zone metamorphism, and tectonic exhumation along the East Asian continental margin. Annu. Rev. Earth Planet. Sci. 35, 73–110.

Eide, E.A., Mcwilliams, M.O., Liou, J.G., 1994. ^{40}Ar/^{39}Ar geochronology and exhumation of high-pressure to ultrahigh-pressure metamorphic rocks in east central China. Geology 22, 601–604.

Gebauer, D., Schertl, H.-P., Brix, M., Schreyer, W., 1997. 35 Ma old ultrahigh-pressure metamorphism and evidence for very rapid exhumation in the Dora Maira Massif, Western Alps. Lithos 41, 5–24.

Hacker, B.R., Wang, X., Eide, E.A., Ratschbacher, L., 1996. The Qinling–Dabie ultra-high-pressure collisional orogen. In: Yin, A., Harrison, M.T. (Eds.), The Tectonic Evolution of Asia. Cambridge University Press, Cambridge, pp. 345–370.

Hacker, B.R., Ratschbacher, L., Webb, L.E., Ireland, T., Walker, D., Dong, S., 1998. Zircon ages constrain the architecture of the ultrahigh-pressure Qinling–Dabie orogen, China. Earth Planet. Sci. Lett. 161, 215–230.

Hacker, B.R., Ratschbacher, L., Webb, L.E., McWilliams, M.O., Ireland, T., Calvert, A., Dong, S., Wenk, H.-R., Chateigner, D., 2000. Exhumation of ultrahigh-pressure continental crust in east central China: Late Triassic–Early Jurassic tectonic unroofing. J. Geophys. Res. 105, 13,339–13,364.

Hacker, B.R., Wallis, S.R., Ratschbacher, L., Grove, M., Gehrels, G., 2006. High-temperature geochronology constraints on the tectonic history and architecture of the ultrahigh-pressure Dabie–Sulu Orogen. Tectonics 25, TC5006. doi:10.1029/2005TC001937.

Hames, W.E., Bowring, S.A., 1994. An empirical evaluation of the argon diffusion geometry in muscovite. Earth Planet. Sci. Lett. 124, 161–167.

Hoskin, P.W.O., Black, L.P., 2000. Metamorphic zircon formation by solid-state recrystallization of protolith igneous zircon. J. Metam. Geol. 18, 423–439.

Hu, N., Zhao, D., Xu, B., Wang, T., 1995. Petrography and metamorphism study on high-ultrahigh pressure eclogite from Guanpo area, northern Qinling Mountains. J. Mineral. Petrol. 15, 1–9 (in Chinese with English abstract).

Hu, N., Yang, J., Zhao, D., 1996. Sm/Nd isochron age of eclogite from northern Qinling Mountains. Acta Mineral. Sin. 16, 349–352 (in Chinese with English abstract).

Jahn, B.-M., Caby, R., Monie, P., 2001. The oldest UHP eclogites of the world: age of UHP metamorphism, nature of protoliths and tectonic implications. Chem. Geol. 178, 143–158.

Jahn, B.-M., Liu, X., Yui, T.-F., Morin, N., Coz, B.-L.M., 2005. High-pressure/ultrahigh-pressure eclogites from the Hong'an Block, east-central China: geochemical characterization, isotope disequilibrium and geochronological controversy. Contrib. Mineral. Petrol. 149, 499–526.

Jian, P., Yang, W., Li, Z., 1997. Isotopic geochronological evidence for the Caledonian Xiongdian eclogite in the western Dabie Mountains, China. Acta Geol. Sin. 71, 133–141 (in Chinese with English abstract).

Jian, P., Liu, D., Yang, W., Williams, I.S., 2000. Petrographical study of zircons and SHRIMP dating of the Caledonian Xiongdian eclogite, northwestern Dabie Mountains. Acta Geol. Sin. 74, 259–264 (in Chinese with English abstract).

Kröner, A., Zhang, G.W., Sun, Y., 1993. Granulites in the Tongbai area, Qinling belt, China: geochemistry, petrology, single zircon geochronology, and implications for the tectonic evolution of eastern Asia. Tectonics 12, 245–255.

Leech, M.L., Webb, L.E., Yang, T.N., 2006. Diachronous histories for the Dabie–Sulu orogen from high-temperature geochronology. In: Hacker, B.R., McClelland, W.C., Liou, J.G. (Eds.), Ultrahigh-Pressure Metamorphism: Deep Continental Subduction, Geological Society of America Special Paper, 403, pp. 1–22.

Li, S., Huang, F., Nie, Y., Han, W., Long, C., Li, H., Zhang, S., Zhang, Z., 2001. Geochemical and Geochronological constraints on the suture location between the North and South China Blocks in the Dabie orogen, central China. Phys. Chem. Earth (A) 26, 655–672.

Li, X.P., Zheng, Y.F., Wu, Y.B., Chen, F.K., Gong, B., Li, Y.L., 2004. Low-T eclogite in the Dabie terrane of China: petrological and isotopic constraints on fluid activity and radiometric dating. Contrib. Mineral. Petrol. 148, 443–470.

Li, Z.X., Li, X.H., Kinny, P.D., Wang, J., Zhang, S., Zhou, H., 2003. Geochronology of Neoproterozoic syn-rift magmatism in the Yangtze Craton, South China and correlations with other continents: evidence for a mantle superplume that broke up Rodinia. Precambrian Res. 122, 85–109.

Liermann, H.-P., Isachsen, C., Altenberger, U., Oberhänsli, R., 2002. Behavior of zircon during high-pressure, low-temperature metamorphism: case study from the Internal Unit of the Sesia Zone (Western Italian Alps). Eur. J. Mineral. 14, 61–71.

Ling, W.L., Gao, S., Zhang, B.R., Zhou, L., Xu, Q.D., 2001. The recognizing of ca. 1.95 Ga tectono-thermal event in Kongling nucleus and its significance for the evolution of Yangtze Block, South China. Chinese Sci. Bull. 46, 326–329.

Liou, J.G., Zhang, R.Y., Wang, X., Eide, E.A., Ernst, W.G., Maruyama, S., 1996. Metamorphism and tectonics of high-pressure and ultra-high-pressure belts in

Fig. 8. ^{40}Ar/^{39}Ar plateau age spectra and inverse isochron plots for muscovites from quartzofeldspathic orthogneiss (samples HYH01-11, GM02-4 and GJZ10-1), feldspathic quartzite (sample DFS06-1) and quartzofeldspathic paragneiss (sample SHZ03-5) in the Tongbaishan area.

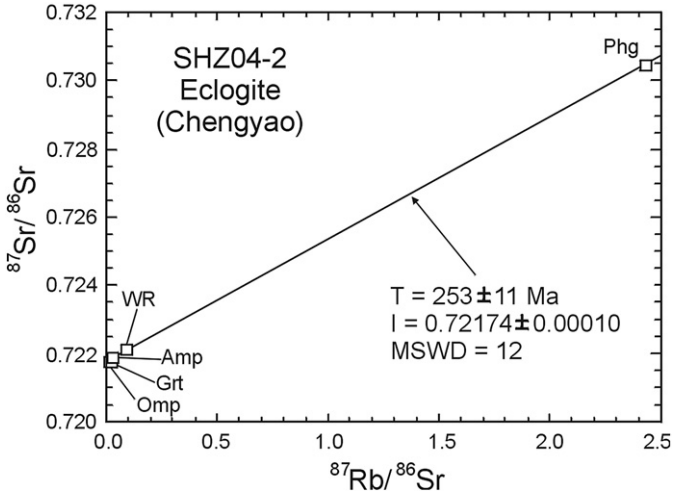

Fig. 10. Phengite-based Rb–Sr isochron diagram for the Chengyao eclogite (sample SHZ04-2) from the Tongbaishan area.

the Dabie–Sulu region, China. In: Yin, A., Harrison, M.T. (Eds.), The Tectonic Evolution of Asia. Cambridge University Press, Cambridge, pp. 300–344.

Liu, X., Jahn, B.-M., Dong, S., Li, H., Oberhänsli, R., 2003. Neoproterozoic granitoid did not record ultrahigh-pressure metamorphism from the southern Dabieshan of China. J. Geol. 111, 719–732.

Liu, X., Jahn, B.-M., Liu, D., Dong, S., Li, S., 2004a. SHRIMP U–Pb zircon dating of a metagabbro and eclogites from western Dabieshan (Hong'an block), China, and its tectonic implications. Tectonophysics 394, 171–192.

Liu, X., Wei, C., Li, S., Dong, S., Liu, J., 2004b. Thermobaric structure of a traverse across western Dabieshan: implications for collision tectonics between the Sino-Korean and Yangtze cratons. J. Metam. Geol. 22, 361–379.

Liu, X., Lou, Y., Dong, S., 2005. *P–T* path of low-temperature eclogites from the Tongbaishan area. Acta Petrol. Sin. 21, 1081–1093 (in Chinese with English abstract).

Liu, F.L., Gerdes, A., Liou, J.G., Xue, H.M., Liang, F.H., 2006a. SHRIMP U–Pb zircon dating from Sulu–Dabie dolomitic marble, eastern China: constraints on prograde, ultrahigh-pressure and retrograde metamorphic ages. J. Metam. Geol. 24, 569–589.

Liu, D., Jian, P., Kröner, A., Xu, S., 2006b. Dating of prograde metamorphic events deciphered from episodic zircon growth in rocks of the Dabie–Sulu UHP complex, China. Earth Planet. Sci. Lett. 250, 650–666.

Lo, C.H., Onstott, T.C., 1989. ^{39}Ar recoil artifacts in chloritized biotite. Geochim. Cosmochim. Acta 53, 2697–2711.

Ludwig, K.R., 1999. Isoplot/Ex (v. 2.06)—a geochronological toolkit for Microsoft Excel. Berkeley Geochronology Center, Special Publication, No. 1a.

Ludwig, K.R., 2001a. SQUID 1.02: a user's manual. Berkeley Geochronology Center, Special Publication, No. 2.

Ludwig, K.R., 2001b. Users manual for Isoplot/Ex v. 2.49: a geochronological toolkit for Microsoft Excel. Berkeley Geochronology Center, Special Publication, No. 1a.

Okay, A.I., Sengör, A.M.C., Satir, M., 1993. Tectonics of an ultrahigh-pressure metamorphic terrane: the Dabie Shan/Tongbai Shan orogen, China. Tectonics 12, 1320–1334.

Qiu, Y.M., Gao, S., McNaughton, N.J., Groves, D.I., Ling, W.L., 2000. First evidence of >3.2 Ga continental crust in the Yangtze craton of south China and its implications for Archean crust evolution and Phanerozoic tectonics. Geology 28, 11–14.

Ratschbacher, L., Hacker, B.R., Calvert, A., Webb, L.E., Grimmer, J.C., Mcwilliams, M.O., Ireland, T., Dong, S., Hu, J., 2003. Tectonics of the Qinling (Central China): tectonostratigraphy, geochronology, and deformation history. Tectonophysics 366, 1–53.

Ratschbacher, L., Franz, L., Enkelmann, E., Jonckheere, R., Pörschke, A., Hacker, B.R., Dong, S., Zhang, Y., 2006. The Sino-Korean-Yangtze suture, the Huwan detachment, and the Paleozoic–Tertiary exhumation of (ultra)high-pressure rocks along the Tongbai–Xinxian–Dabie Mountains. In: Hacker, B.R., McClelland, W.C., Liou, J.G. (Eds.), Ultrahigh-Pressure Metamorphism: Deep Continental Subduction, Geological Society of America Special Paper, 403, pp. 45–75.

Rowley, D.B., Xue, F., Tucker, R.D., Peng, Z.X., Baker, J., Davis, A., 1997. Ages of ultrahigh pressure metamorphism and protolith orthogneisses from the eastern Dabie Shan: U/Pb zircon geochronology. Earth Planet. Sci. Lett. 151, 191–203.

Rubatto, D., Gebauer, D., Fanning, M., 1998. Jurassic formation and Eocene subduction of the Zermatt–Saas–Fee ophiolites: implications for the geodynamic evolution of the Central and Western Alps. Contrib. Mineral. Petrol. 132, 269–287.

Rubatto, D., Gebauer, D., Compagnoni, R., 1999. Dating of eclogite-facies zircons: the age of Alpine metamorphism in the Sesia-Lanzo Zone (Western Alps). Earth Planet. Sci. Lett. 167, 141–158.

Rubatto, D., Gebauer, D., 2000. Use of cathodoluminescence for U–Pb zircon dating by ion microprobe; some examples from the Western Alps. In: Pagel, M., Barbin, V., Blanc, P., Ohnenstetter, D. (Eds.), Cathodoluminescence in geosciences. Springer, Berlin, pp. 373–400.

Sun, W., Williams, I.S., Li, S., 2002. Carboniferous and Triassic eclogites in the western Dabie Mountains, east-central China: evidence for protracted convergence of the North and South China Blocks. J. Metam. Geol. 20, 873–886.

Suo, S., Zhong, Z., Zhang, H., Zhou, H., You, Z., 2001. High-pressure metamorphic belt and its tectonic pattern in Tongbai Mountains, central China. Earth Sci. 26, 551–559 (in Chinese with English abstract).

Tang, J., Zheng, Y.F., Wu, Y.B., Zha, X.P., Zhou, J.B., 2004. Zircon U–Pb ages and oxygen isotopes of high-grade metamorphic rocks in the eastern part of the Shandong Peninsula. Acta Petrol. Sin. 20, 1039–1062 (in Chinese with English abstract).

Wan, Y., Li, R., Wilde, S.A., Liu, D., Chen, Z., Yan, L., Song, T., Yin, X., 2005. UHP metamorphism and exhumation of the Dabie Orogen, China: evidence from SHRIMP dating of zircon and monazite from a UHP granitic gneiss cobble from the Hefei Basin. Geochim. Cosmochim. Acta 69, 4333–4348.

Webb, L.E., Hacker, B.R., Ratschbacher, L., McWilliams, M.O., Dong, S., 1999. Thermochronologic constraints on deformation and cooling history of high- and ultrahigh-pressure rocks in the Qinling–Dabie orogen, eastern China. Tectonics 18, 621–638.

Webb, L.E., Ratschbacher, L., Hacker, B.R., Dong, S., 2001. Kinematics of exhumation of high- and ultrahigh-pressure rocks in the Hong'an and Tongbai Shan of the Qinling–Dabie collisional orogen, eastern China. In: Hendrix, M.S., Davis, G.A. (Eds.), Paleozoic and Mesozoic Tectonic Evolution of Central Asia: from Continental Assembly to Intracontinental Deformation, Memoir 194. Geological Society of America, Boulder, Colorado, pp. 231–245.

Webb, L.E., Leech, M.L., Yang, T.N., 2006. ^{40}Ar/^{39}Ar thermochronology of the Sulu terrane: late Triassic exhumation of high- and ultrahigh-pressure rocks and implications for Mesozoic tectonics in East Asia. In: Hacker, B.R., McClelland, W.C., Liou, J.G. (Eds.), Ultrahigh-Pressure Metamorphism: Deep Continental Subduction, Geological Society of America Special Paper, 403, pp. 77–92.

Wei, C., Wu, Y., Ni, Y., Chen, B., Wang, S., Chang, Z., 1999. Characteristics of eclogite from Tongbai area, Henan peovince, and its geological significance. Chin. Sci. Bull. 44, 1882–1885 (in Chinese).

Williams, I.S., 1998. U–Th–Pb geochronology by ion microprobe. In: McKibben, M.A., Shanks, W.C., Ridley, W.I. (Eds.), Applications of Microanalytical Techniques to Understanding Mineralizing Processes. Rev. Econ. Geol., 7, pp. 1–35.

Williams, I.S., Claesson, S., 1987. Isotopic evidence for the Precambrian provenance and Caledonian metamorphism of high grade paragneisses from the Seve Nappes, Scandinavian Caledonides. II. Ion microprobe zircon U–Th–Pb. Contrib. Mineral. Petrol. 97, 205–217.

Wu, Y.B., Zheng, Y.F., Zhao, Z.F., Gong, B., Liu, X.M., Wu, F.Y., 2006. U–Pb, Hf and O isotopes evidence for two episodes of fluid-assisted zircon growth in marble-hosted eclogites from the Dabie Orogen. Geochim. Cosmochim. Acta 70, 3743–3761.

Wu, Y.B., Gao, S., Zhang, H.F., Yang, S.H., Jiao, W.F., Liu, Y.S., Yuan, H.L., 2008. Timing of UHP metamorphism in the Hong'an area, western Dabie Mountains, China: evidence from zircon U–Pb age, trace element and Hf isotope composition. Contrib. Mineral. Petrol. 155, 123–133.

Xu, B., Grove, M., Wang, C., Zhang, L., Liu, S., 2000. ^{40}Ar/^{39}Ar thermochronology from the northwestern Dabie Shan: constraints on the evolution of Qinling–Dabie orogenic belt, east-central China. Tectonophysics 322, 279–301.

Xue, F., Rowley, D.B., Tucker, R.D., Peng, Z., 1997. U–Pb zircon ages of granitoid rocks in the north Dabie Complex, eastern Dabie Shan, China. J. Geol. 105, 744–753.

Yang, J.S., Xu, Z.Q., Dobrzhinetskaya, L.F., Green II, H.W., Pei, X.Z., Shi, R.D., Wu, C.L., Wooden, J., Zhang, J.X., Wan, Y.S., Li, H.B., 2003a. Discovery of metamorphic diamonds in central China: an indication of a >4000-km-long zone of deep subduction resulting from multiple continental collisions. Terra Nova 15, 370–379.

Yang, J.S., Wooden, J.L., Wu, C.L., Liu, F.L., Xu, Z.Q., Shi, R.D., Katayama, I., Liou, J.G., Maruyama, S., 2003b. SHRIMP U–Pb dating of coesite-bearing zircon from the ultrahigh-pressure metamorphic rocks, Sulu terrane, east China. J. Metam. Geol. 21, 551–560.

Zhai, X., Day, H.W., Hacker, B.R., You, Z., 1998. Paleozoic metamorphism in the Qinling orogen, Tongbai Mountains, central China. Geology 26, 371–374.

Zhang, S.B., Zheng, Y.F., Wu, Y.B., Zhao, Z.F., Gao, S., Wu, F.Y., 2006a. Zircon U–Pb age and Hf–O isotope evidence for Paleoproterozoic metamorphic event in South China. Precambrian Res. 151, 265–288.

Zhang, S.B., Zheng, Y.F., Wu, Y.B., Zhao, Z.F., Gao, S., Wu, F.Y., 2006b. Zircon U–Pb age and Hf isotope evidence for 3.8 Ga crustal remnant and episodic reworking of Archean crust in South China. Earth Planet. Sci. Lett. 252, 56–71.

Zhao, G.C., Sun, M., Wilde, S.A., Guo, J.H., 2004. Late Archean to Palaeoproterozoic evolution of the Trans-North China Orogen: insights from synthesis of existing data from the Hengshan-Wutai-Fuping belt. In: Malpas, J., Fletcher, C.J.N., Ali, J.R., Aitchison, J.C. (Eds.), Aspects of the Tectonic Evolution of China. Geological Society, London, Special Publications, 226, 27–55.

Zheng, Y.F., Wu, Y.B., Chen, F.K., Gong, B., Zhao, Z.F., 2004. Zircon U–Pb and oxygen isotope evidence for a large-scale ^{18}O depletion event in igneous rocks during the Neoproterozoic. Geochim. Cosmochim. Acta 68, 4145–4165.

Zheng, Y.F., Zhao, Z.F., Wu, Y.B., Zhang, S.B., Liu, X.M., Wu, F.Y., 2006. Zircon U–Pb age, Hf and O isotope constraints on protolith origin of ultrahigh-pressure eclogite and gneiss in the Dabie orogen. Chem. Geol. 231, 135–158.

Zhong, Z., Suo, S., You, Z., 1999. Regional-scale extensional tectonic pattern of ultrahigh-P and high-P metamorphic belts from the Dabie massif, China. Inter. Geol. Rev. 41, 1,033–1,041.

Zhong, Z., Suo, S., You, Z., Zhang, H., Zhou, H., 2001. Major constituents of the Dabie collisional orogenic belt and partial melting in the ultrahigh-pressure unit. Inter. Geol. Rev. 43, 226–236.